(2)

AFOSR-TR- 89-0438

Ohio University

Athens, Ohio

AN EXPERIMENTAL INVESTIGATION OF

HIGH LIFT/HIGH RATE AERODYNAMICS

OF AN UNSTEADY AIRFOIL

(Grant AFOSR-87-0312)

Department of

Mechanical Engineering

UNCLASSIFIED

SECURITY CLASSIFICATION OF THIS PAGE

A206964 (2)

REPORT DOCUMENTATION PAGE

Form Approved OMB No. 0704-0188

1a. REPORT SECURITY CLASSIFICATION UNCLASSIFIED	1b. RESTRICTIVE MARKINGS
2a. SECURITY CLASSIFICATION AUTHORITY	3. DISTRIBUTION/AVAILABILITY OF REPORT APPROVED FOR PUBLIC RELEASE DISTRIBUTION IS UNLIMITED
2b. DECLASSIFICATION/DOWNGRADING SCHEDULE	
4. PERFORMING ORGANIZATION REPORT NUMBER(S)	5. MONITORING ORGANIZATION REPORT NUMBER(S) AFOSR-TR- 89 0438
6a. NAME OF PERFORMING ORGANIZATION OHIO UNIVERSITY 6b. OFFICE SYMBOL (If applicable)	7a. NAME OF MONITORING ORGANIZATION AFOSR/NA
6c. ADDRESS (City, State, and ZIP Code) MECHANICAL ENGINEERING ATHENS, OHIO 45701-2979	7b. ADDRESS (City, State, and ZIP Code) BUILDING 410 BOLLING AFB, DC 20332-6448
8a. NAME OF FUNDING/SPONSORING ORGANIZATION AFOSR 8b. OFFICE SYMBOL (If applicable) NA	9. PROCUREMENT INSTRUMENT IDENTIFICATION NUMBER AFOSR-87-0312
8c. ADDRESS (City, State, and ZIP Code) BUILDING 410 BOLLING AFB, DC 20332-6448	10. SOURCE OF FUNDING NUMBERS PROGRAM ELEMENT NO. 61102F; PROJECT NO. 2307; TASK NO. A3; WORK UNIT ACCESSION NO.

11. TITLE (Include Security Classification)

(U) AN EXPERIMENTAL INVESTIGATION OF HIGH LIFT/HIGH RATE AERODYNAMICS

12. PERSONAL AUTHOR(S)

G.M. GRAHAM

13a. TYPE OF REPORT	13b. TIME COVERED	14. DATE OF REPORT (Year, Month, Day)	15. PAGE COUNT
FINAL REPORT	FROM 15 Sep 87 TO 31 Dec 88	MAR 1989	47

16. SUPPLEMENTARY NOTATION

17. COSATI CODES			18. SUBJECT TERMS (Continue on reverse if necessary and identify by block number)
FIELD	GROUP	SUB-GROUP	UNSTEADY AERODYNAMICS, PITCHING AIRFOILS, MANEUVERABILITY

19. ABSTRACT (Continue on reverse if necessary and identify by block number)

An experimental study of a two dimensional NACA 0015 airfoil undergoing both positive and negative pitch rate motions in presented. Test results consist of lift and drag force measurements and flow visualizations. The results of this study provide insight into the airfoil-dynamic stall vortex interactions during the ~~pitch~~ Pitch down and cessation of aerodynamic stall.

20. DISTRIBUTION/AVAILABILITY OF ABSTRACT	21. ABSTRACT SECURITY CLASSIFICATION
☐ UNCLASSIFIED/UNLIMITED ☒ SAME AS RPT. ☐ DTIC USERS	UNCLASSIFIED
22a. NAME OF RESPONSIBLE INDIVIDUAL HENRY E. HELIN	22b. TELEPHONE (Include Area Code) 202-767-0471
	22c. OFFICE SYMBOL AFOSR/NA

DD Form 1473, JUN 86 — Previous editions are obsolete. — SECURITY CLASSIFICATION OF THIS PAGE

UNCLASSIFIED

AN EXPERIMENTAL INVESTIGATION OF HIGH LIFT/HIGH RATE AERODYNAMICS OF AN UNSTEADY AIRFOIL

(Grant AFOSR-87-0312)

FINAL REPORT

Submitted To

THE AFOSR

Washington, D.C. 20332

by

G.M. Graham

Ohio University

Athens, Ohio 45701

March 1989

Summary

An experimental study of a two dimensional NACA 0015 airfoil undergoing both positive and negative constant pitch rate motions at high angles of attack has been conducted in the Ohio University tow tank facility. Nondimensional pitch rates ($K = \dot{\alpha}C/2U_\infty$) in the range of $0.1 < K < 0.7$ and Reynolds numbers in the range of $141{,}000 < Re < 342{,}000$ were considered. Test results consist of lift and drag force coefficients and flow visualizations. The results of this study provide insight into the airfoil-dynamic stall vortex interaction during the pitch down motion and the cessation of aerodynamic stall. These data may be useful in high angle of attack applications such as the enhanced maneuverability concept for fighter aircraft.

Table of Contents

Page

1. Introduction.....1

2. Experimental Methods.....1

   2.1 Tow Tank
   2.2 Force Measurement
   2.3 Flow Visualization

3. Results and Discussion.....4

   3.1 Force Coefficients
   3.2 Effect of Pitching Rate
   3.3 Recovery Of Static Lift at the End of Pitch Down
   3.4 Effect of Pitch Down Inception
   3.5 Effect of Reynolds Number
   3.6 Flow Visualizations
   3.7 Flow Reattachment
   3.8 Underside Flow

4. Conclusion.....27

5. Acknowledgments.....27

6. References.....27

Appendix: Lift and Drag Force Data.....30

1. Introduction

Interest in the development of aircraft with enhanced maneuverability at high angles of attack has led to a number of experimental studies of unsteady airfoils experiencing aerodynamic stall. At the root of the enhanced maneuverability concept is the dynamic augmentation of airfoil loading which accompanies rapid pitching motion up to , and beyond the dynamic stall threshold. Much of the experimental work related to this problem has focused on wind tunnel and tow tank testing of constant pitch rate motion from a low to a high angle of attack. Recent studies include the work of Lorber and Carta[1], Jumper et al.[2], Strickland and Graham[3], and Walker et al[4]. These studies encompass a range of Reynolds numbers given by $4.8 \times 10^4 < Re < 4 \times 10^6$ and nondimensional pitching rates($K = \dot{\alpha}C/2U_\infty$) in the range of $.001 < K < 1.0$. Other efforts are given in the review of dynamic stall research by Carr[5]. As envisioned by Herbst[6], a complete post stall maneuver would involve a controlled pitch up motion to a large angle of attack, a period of constant angle of attack motion, followed by a pitch down motion returning to a conventional flight regime. This report describes the findings of a tow tank study of a two dimensional airfoil undergoing such a motion. The present study is one of first to investigate this complete flightpath.

2.Experimental Methods

2.1 Tow Tank

The Ohio University tow tank facility is an above ground tank with a length of 32 ft, a width of 15 ft, and a water depth of 4 ft. As shown in Figure 1, the drive train consists of two I beams which span the length of the tank. The airfoil section is suspended vertically from a carriage which moves along the beams via precision roller bearings. The translational motion is imparted by a 3 hp electric motor and cable drive assembly. In the present study a 14 inch chord NACA 0015 airfoil was towed at three Reynolds numbers of 141,000, 248,000 and 342,000. The pitching motion is driven by a 3 hp stepper motor which is mounted on the carriage. The stepper motor is connected to the airfoil drive shaft through a 10 to 1 speed reducer. The stepper motor motion is controlled by software commands from an IBM microcomputer which is located beside the tank. The microcomputer also performs the data acquisition. The stepper motor can impart both pitching up and pitching down motions. In the present study the angle of attack was varied as shown in Figure 2. These data were acquired using a rotational potentiometer mounted on the airfoil drive shaft for $K = 0.2$. As seen in Figure 2, the airfoil motion consists of an initial motion at 0 degrees alpha for a distance of 3 chord lengths, a ramp-up at constant rate to 90 degrees, a motion at 90 degrees for a distance of 0.25 chord lengths, a ramp-down to 0 degrees alpha, and a final motion at 0 degrees alpha to the end of the tow tank. The nondimensional

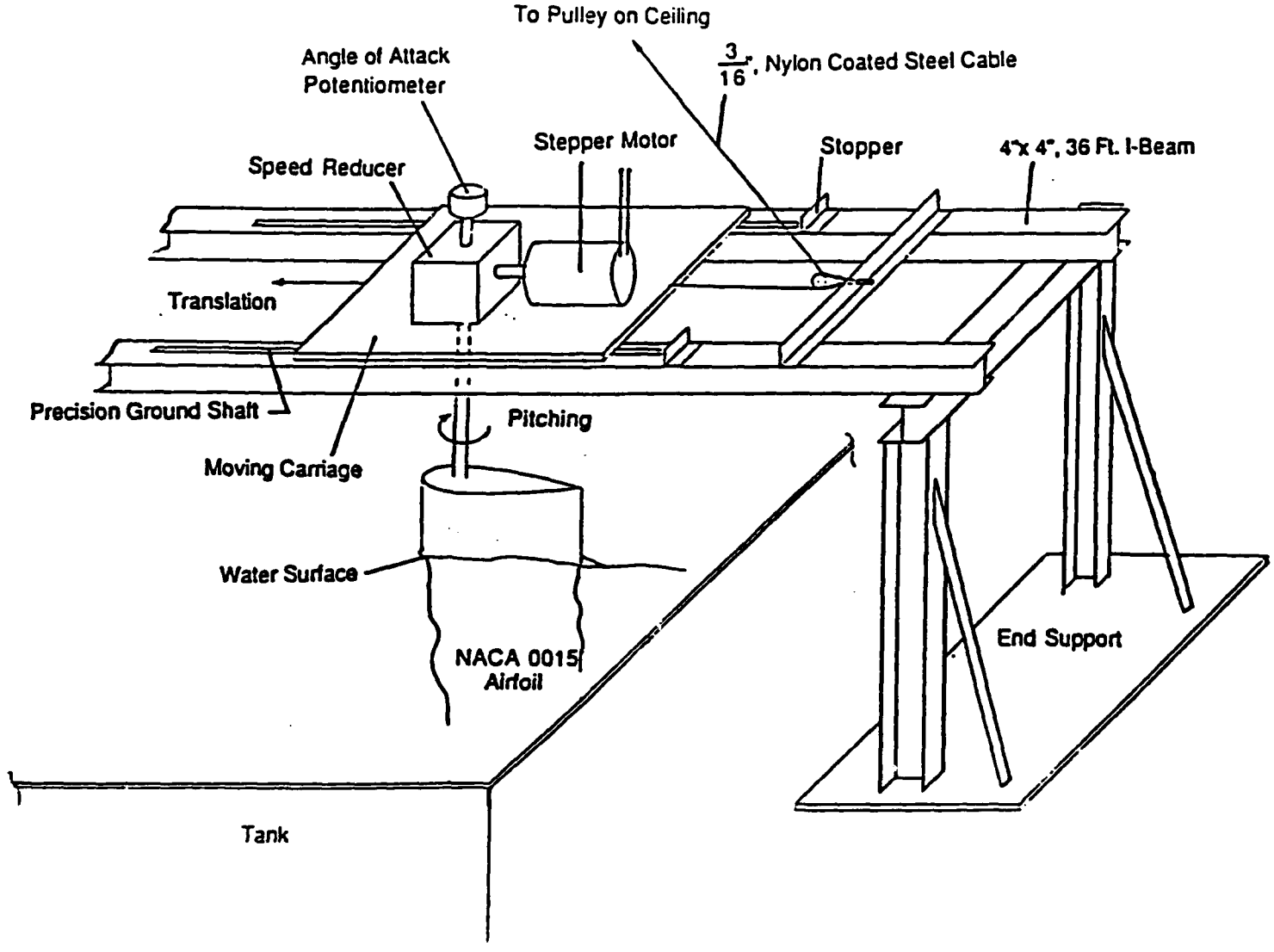

Figure 1. Tow Tank Facility

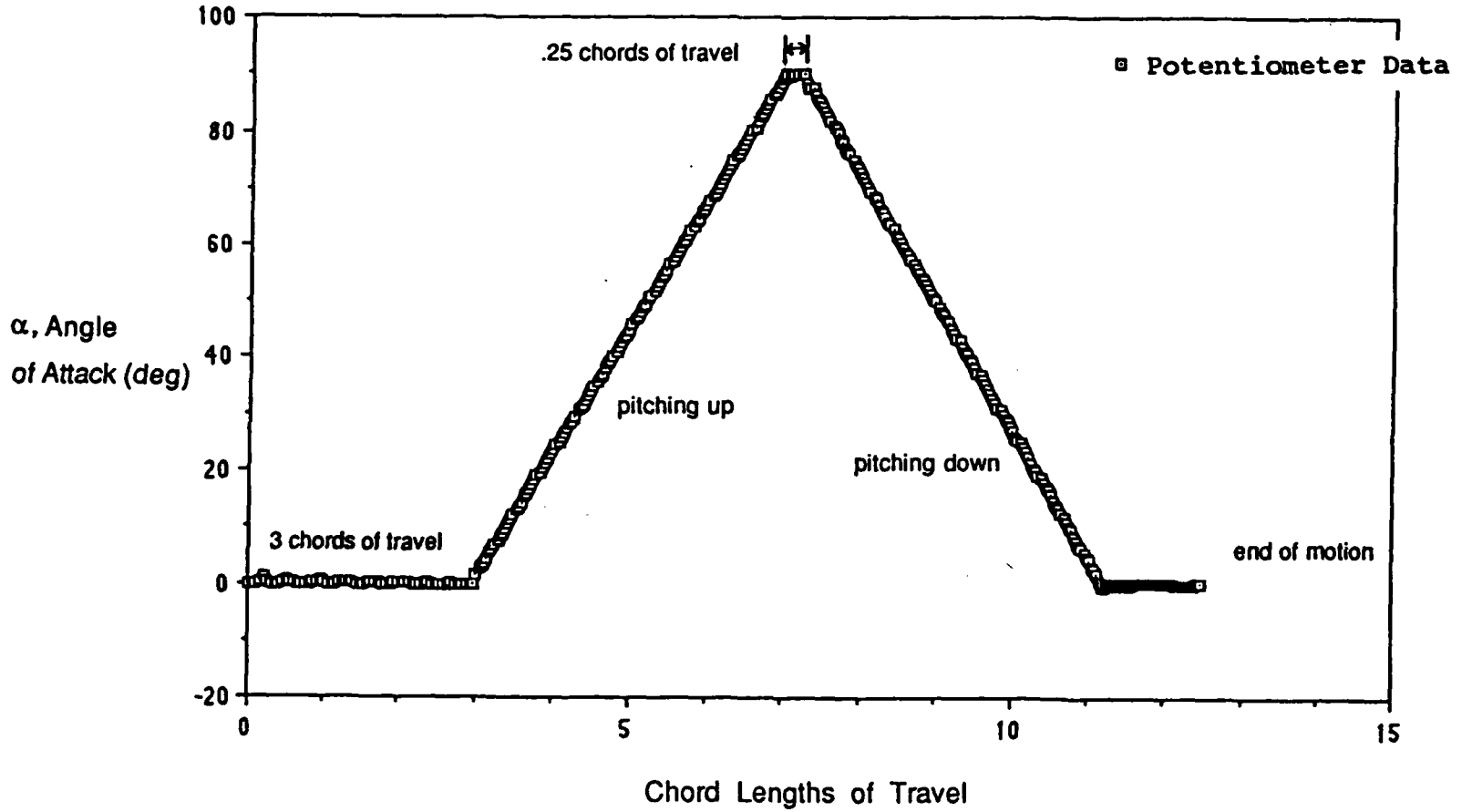

Figure 2. Airfoil Test Motion For K=Ø.2

pitching rate was varied in the range of $0.1 < K < 0.7$. Additional details are available in Reference[7].

2.2 Force Measurements

The normal and tangential forces acting on the airfoil were measured using strain gauges as shown in Figure 3. The gauges are attached to the airfoil drive shaft which is located at the airfoil quarter chord. The gauges are connected in two Wheatstone bridge circuits. Each bridge is sensitive to the desired force only. The axis of the airfoil drive shaft does not coincide with the airfoil section center of mass. Therefore, the signal from the tangential force bridge must be corrected for the inertial loading during pitching. The normal force bridge is not affected by the airfoil inertia. In addition, the drag induced by the free end has been accounted for following the method given in Reference[7]. Both the inertial and induced drag corrections are small. The lift(L) and drag(D) forces are related to the normal(N) and tangential(T) forces by:

$$L = N\cos\alpha + T\sin\alpha$$
$$D = N\sin\alpha - T\cos\alpha \qquad (1)$$

where α is the angle of attack. The lift and drag coefficients are defined by:

$$C_L = L/(1/2\rho U_\infty^2 C1)$$
$$C_D = D/(1/2\rho U_\infty^2 C1) \qquad (2)$$

where 1 is the submerged length of the airfoil section.

2.3 Flow Visualization

The flow visualizations were performed using a hydrogen bubble wire technique shown in Figure 4. The bubble wire is a ladder type probe and is mounted approximately one-half chord length in front of the airfoil. A Cannon 35 mm SLR camera with a high speed winder was used to photograph the flow. Small amounts of hydrogen sulfate were added to the water to increase the bubble production rate. Photographs were taken in the plane of the bubble wire using a submersible mirror to check the two dimensionality of the flow. These visualizations indicated only a minor deviation from a two dimensional flow.

3.Results and Discussion

3.1 Lift and Drag Coefficients

Lift and drag force coefficients were obtained on a NACA 0015 airfoil pitching about the quarter chord for the motion shown in Figure 2. Three Reynolds numbers based on airfoil chord

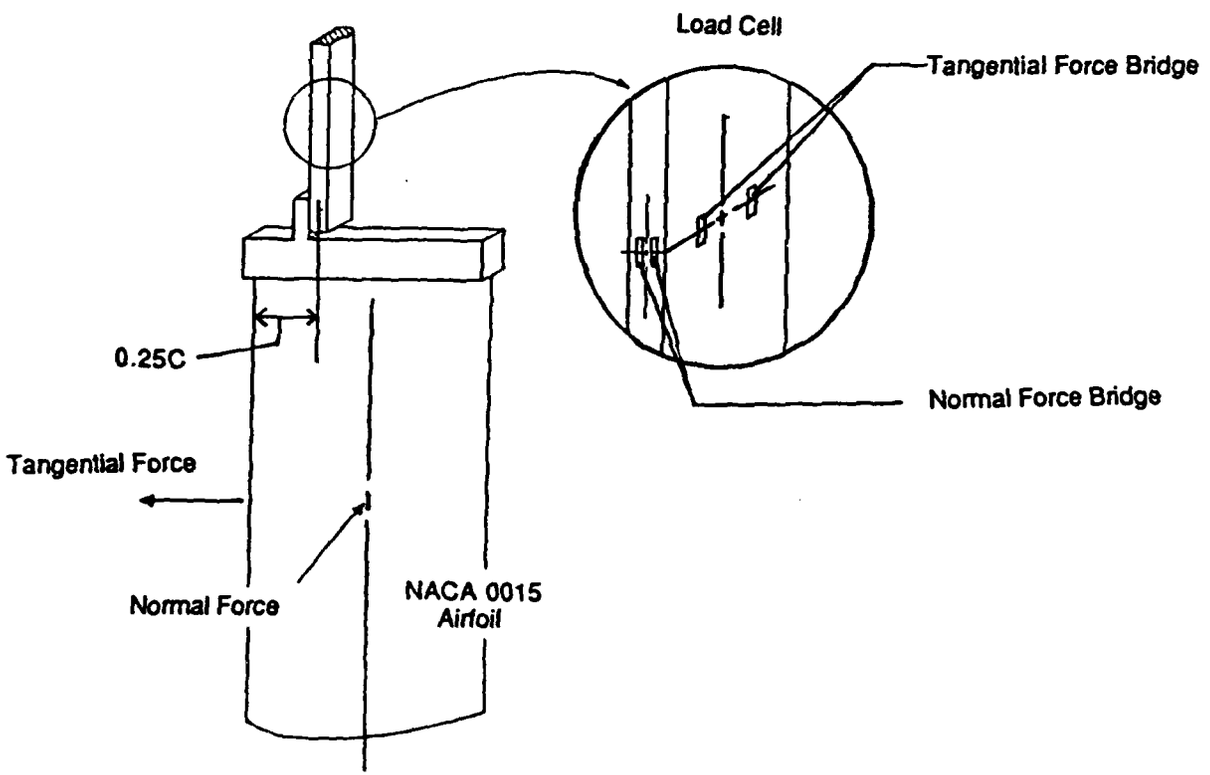

Figure 3. Strain Gauge Load Cell

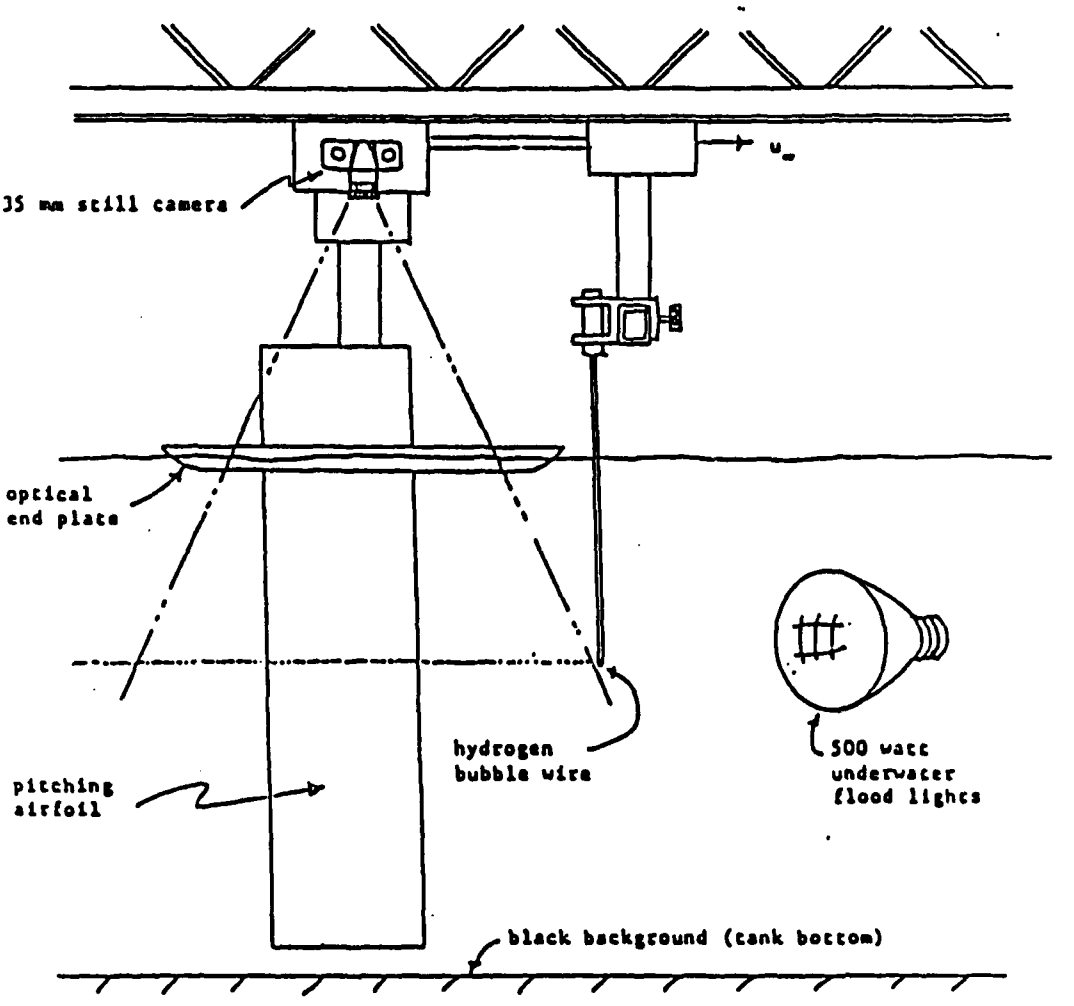

Figure 4. Flow Visualization Set Up

of 141,000, 248,000, and 342,000 were studied. At the two lowest Reynolds numbers the forces were measured at nondimensional pitching rates of K = 0.1, 0.2, 0.3, 0.4, 0.5, 0.6, and 0.7. At the highest Reynolds number measurements were taken at nondimensional pitch rates of K = 0.1, 0.2, and 0.3. Shown in Figures 5 through 7 are representative lift and drag force results for the nondimensional pitch rates of K = 0.1, 0.3, and 0.7 respectively, for a Reynolds number of 248,000. As seen in Figure 5 for the case of K = 0.1, the maximum angle of attack is 55 degrees. The limitation on the maximum angle of attack in this case is due to the finite length of travel in the tow tank. The remainder of the data are for a maximum angle of attack of 90 degrees. The uncertainty in both the lift and drag force data has been estimated to be ± 11 percent. The uncertainty in the angle of attack is believed to be ± 1 degree. At the maximum angle of attack in Figures 5 through 7 there are, in places, several data points superimposed on one another which correspond to the constant angle of attack portion of the motion. These are plotted more clearly in the discussion to follow. In some instances the lift and drag forces are negative just after the inception of the pitching motion near 0 degrees angle of attack. This may be attributed to the inertia of the airfoil during the short period of acceleration to a constant pitch rate. A complete set of lift and drag force data are given in Appendix A.

There are a few generalizations which can be made with regard to the data in Figures 6 and 7. The lift coefficient becomes very small at an angle of attack of 90 degrees. This may be explained by the cosine dependence of the lift on the normal force as given by Equation 1 and by the fact that the tangential force is small compared to the normal force. By the same token, the maximum drag, which is sine dependent on the normal force, tends to occur at 90 degrees. The relative magnitudes of the lift and drag forces are illustrated in Figure 8 where the natural log of the quotient of the lift and drag are plotted as a function of the angle of attack for several pitching rates. For values of alpha where the natural log is negative the drag is the dominant force, and where positive the lift is the dominant load. It is seen that the lift is dominant at lower angles of attack and that the drag is dominant at higher angles of attack. It is interesting to note that even over the very large range of pitching rates plotted here the behavior of the loads are very similar, particularly during the pitching up sequence.

3.2 Effect of Pitching Rate

The lift forces for several pitching rates are plotted as a function of angle of attack in Figure 9. The maximum lift increases with pitching rate in the pitching up motion. There is a large drop in the lift force as the airfoil approaches 90 degrees angle of attack. During the pitching down motion the airfoil does not recover from this loss in lift at pitching rates below K = 0.3. However, at pitching rates above K = 0.3 a significant recovery of lift takes place. One explanation for this is that at the higher pitching rates the dynamic stall vortex remains very close to the airfoil surface as the pitching

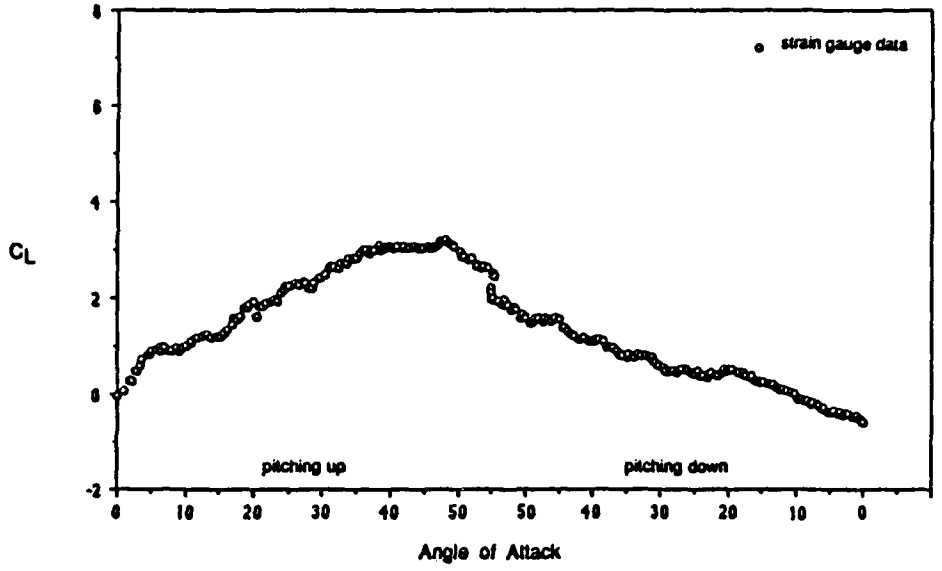

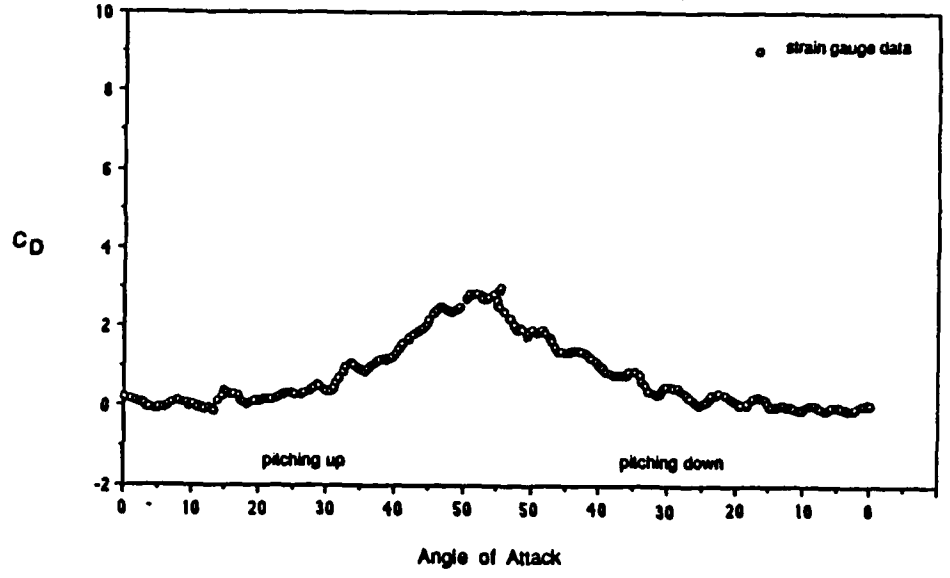

Figure 5. Force Coefficients For K=Ø.1, Re=248,ØØØ

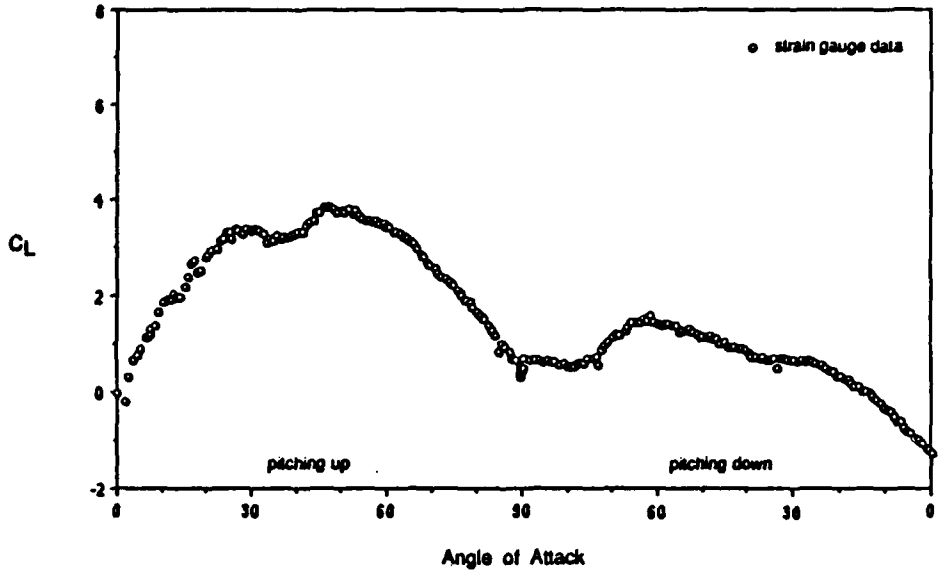

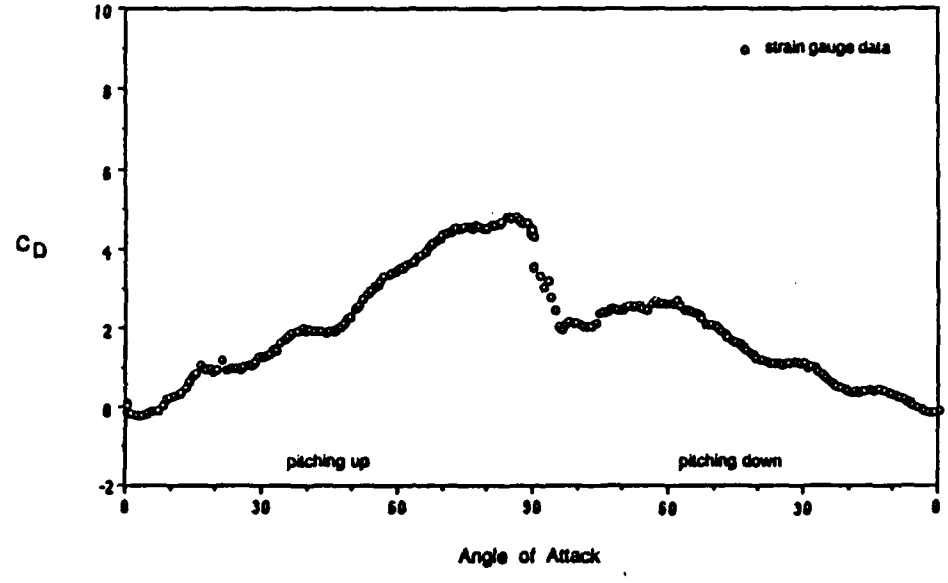

Figure 6. Force Coefficients For K=Ø.3, Re=248,ØØØ

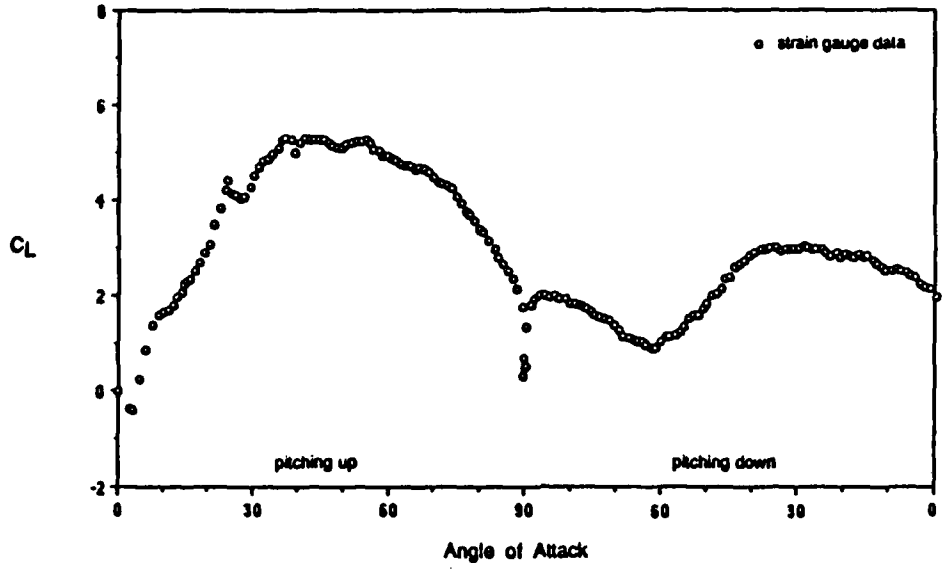

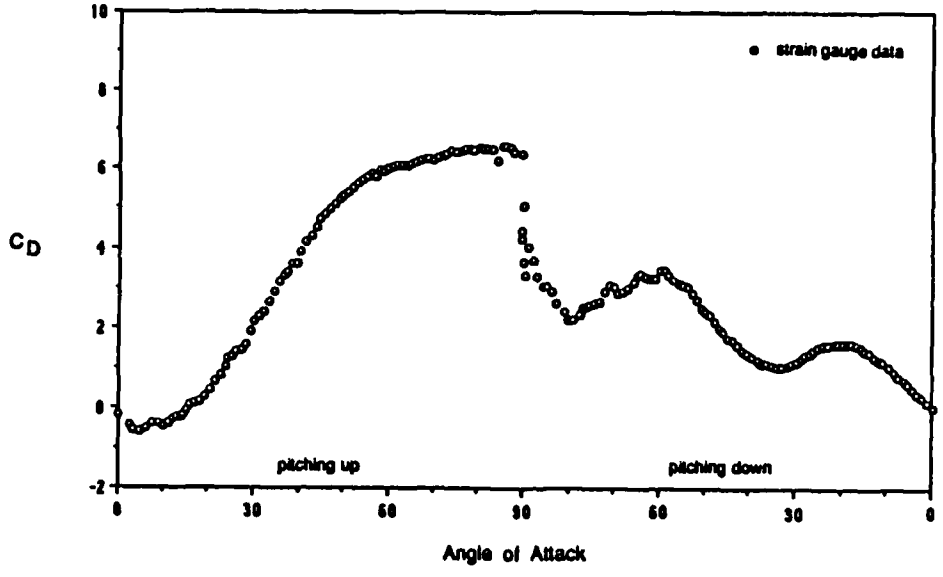

Figure 7. Force Coefficients For K=Ø.7, Re=248,ØØØ

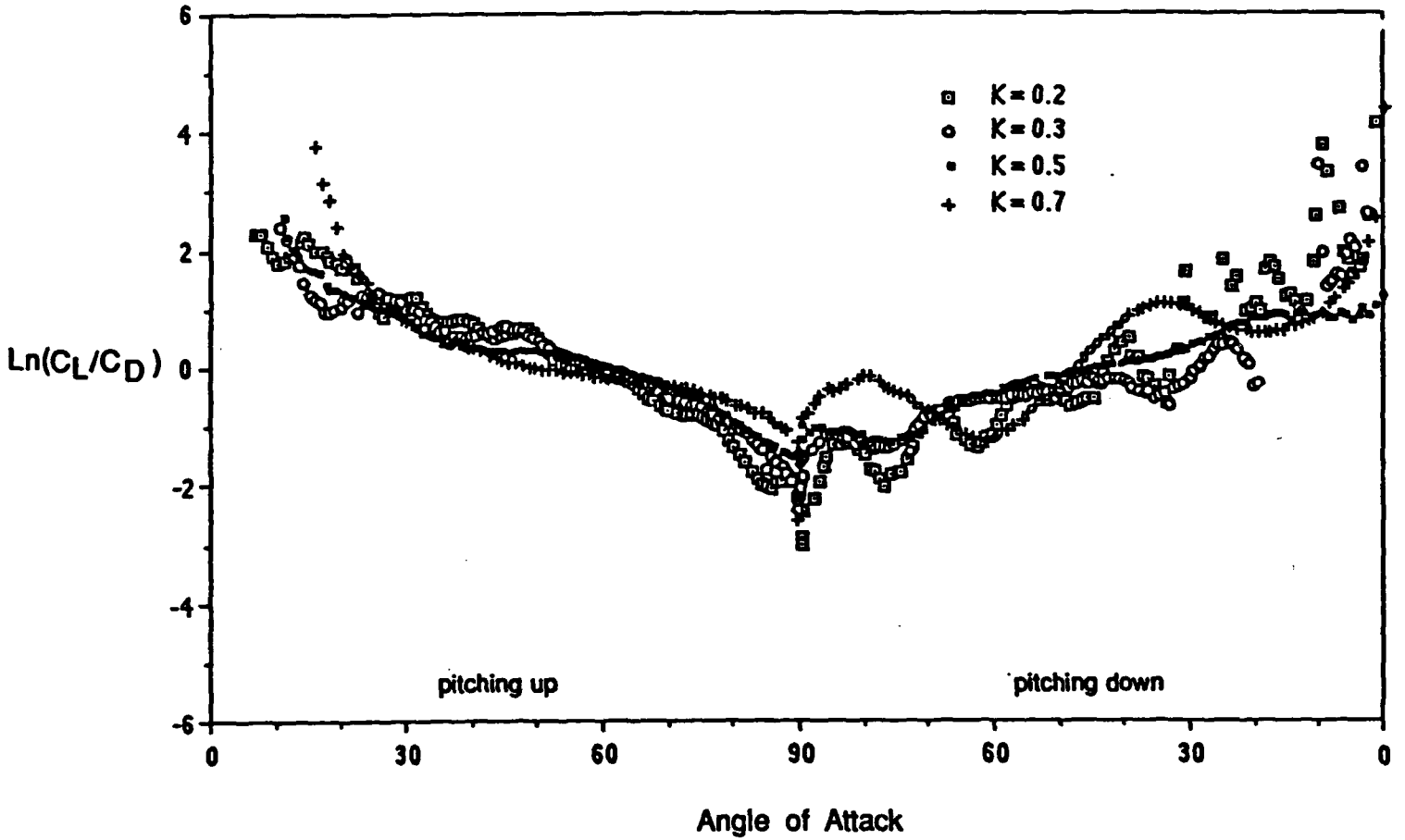

Figure 8. Illustration Of Dominant Forces

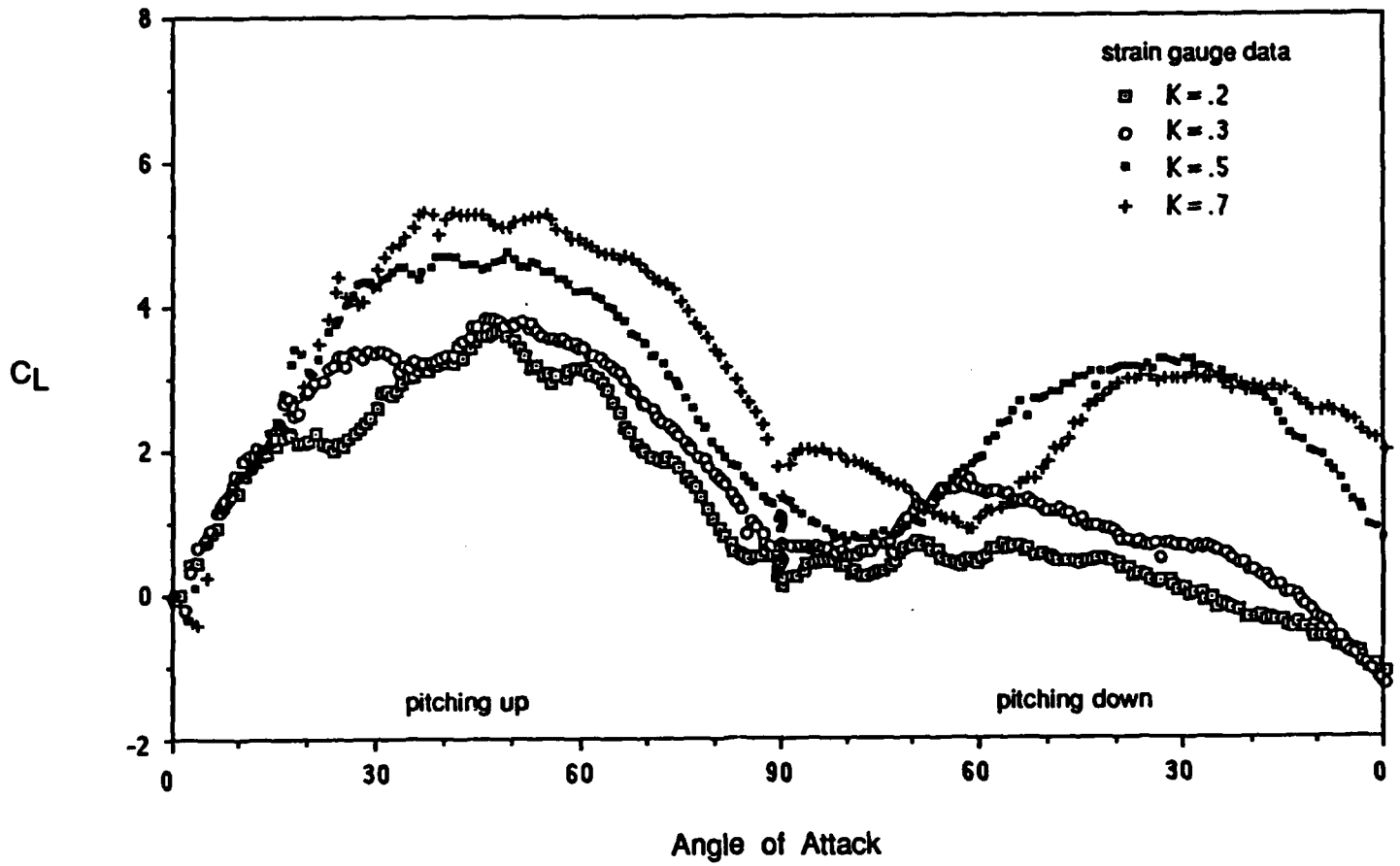

Figure 9. Effect Of Pitching Rate On The Lift For Re=248,000

down motion takes place. In addition, at the high pitching rates the dynamic stall vortex is "tightly wound" and induces very large velocities on the suction side of the airfoil. Furthermore, the diffusion of vorticity is small during the short time duration of the high pitching rate motion. At pitching rates below K = Ø.3 the dynamic stall vortex releases from the airfoil surface and is convected and diffused away as the pitching down motion proceeds. This situation is illustrated in Figure 1Ø which shows the flow for the pitching down motion at two pitching rates of K = Ø.2 and K =Ø.7. As seen in Figure 9, at the end of the pitch down motion there is a large variation in the lift with pitching rate. The return to the static lift from this point is investigated in the Section 3.3.

The effect of pitching rate on the drag force is shown in Figure 11. The maximum drag force increases with increasing pitching rate during the pitching up motion and occurs near 9Ø degrees. At the end of the pitch up sequence there is a large decrease in the drag. With the exception of the case of K=Ø.7, the maximum drag force is directly related to the pitching rate during the pitch down motion. For the case of K = Ø.7 the drag decreases significantly at approximately 35 degrees in the pitch down motion. It is not completely clear what mechanism is at work here, but this may be due to the interaction of the airfoil with the dynamic stall vortex. One possibility is that the strength of the dynamic stall vortex is sufficient to induce a large positive thrust force on the airfoil. As seen in Equation 1, this would cause a reduction in the drag. As the pitch down motion ends the drag at each pitching rate converge to near the same value.

3.3 Recovery of Static Lift at the End of Pitch Down

An unexpected finding of this study was that for pitching rates below K = Ø.4 the lift force becomes negative near the end of the pitch down motion. This can be seen in the data of Figure 9. The lift coefficient at the instant the airfoil reaches Ø degrees angle of attack is plotted as a function of pitch rate in Figure 12. As seen here the lift is negative for pitching rates below K = Ø.4 and is positive for higher pitching rates. The flow visualizations provide some insight into the physical mechanisms which drive the loading at the lower pitching rates. Shown in Figure 13 are the flow visualizations for the case of K = Ø.1. As seen here, as the airfoil angle of attack decreases fluid from the trailing edge initially surges upward and then is forced by the remnants of the dynamic stall vortex downward onto the upper surface of the airfoil. It would appear that the downward momentum of the surging fluid, combined with the negative pitching rate of the airfoil, is sufficient to create a negative normal force and/or lift. The recovery of the static lift is shown in Figure 14. It is seen here that the static lift is achieved during the first 2 chord lengths of travel. This may be of interest in the mathematical modeling of nonlinear aerodynamics using indicial response functions which have been simplified using the concept of the "recent" past[8]. In other words, it would appear in Figure 14 that, to a large extent, it takes about 2 chords of travel for the flow to "forget" what has

K=0.2

α=89° α=74° α=35°

K=0.7

α=89° α=64° α=40°

Figure 10. Flow Visualization Of Dynamic Stall Vortex During Pitch Down Motion For K=0.2 And K=0.7, Re=248,000

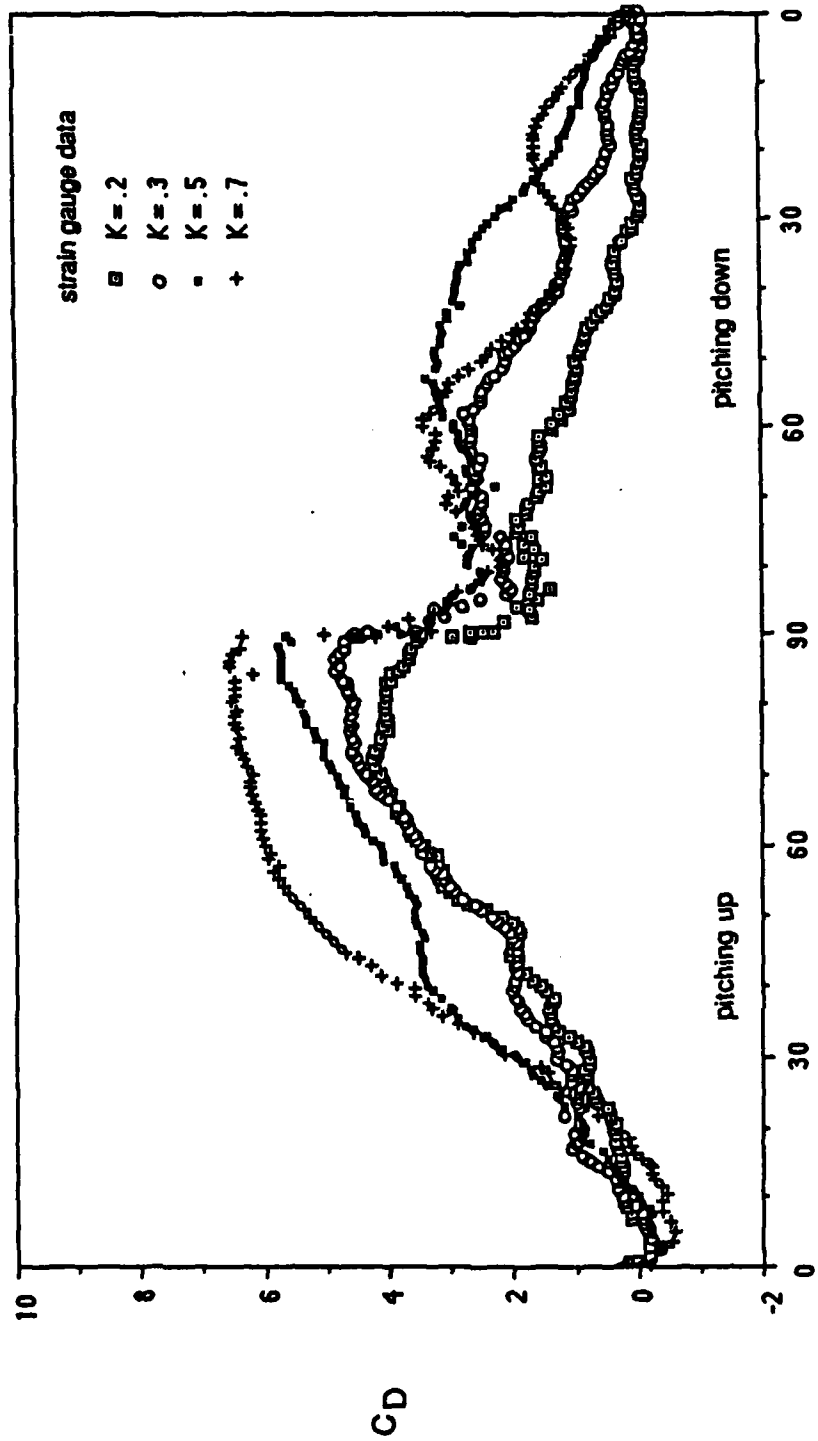

Figure 11. Effect Of Pitching Rate On The Drag For Re=248,000

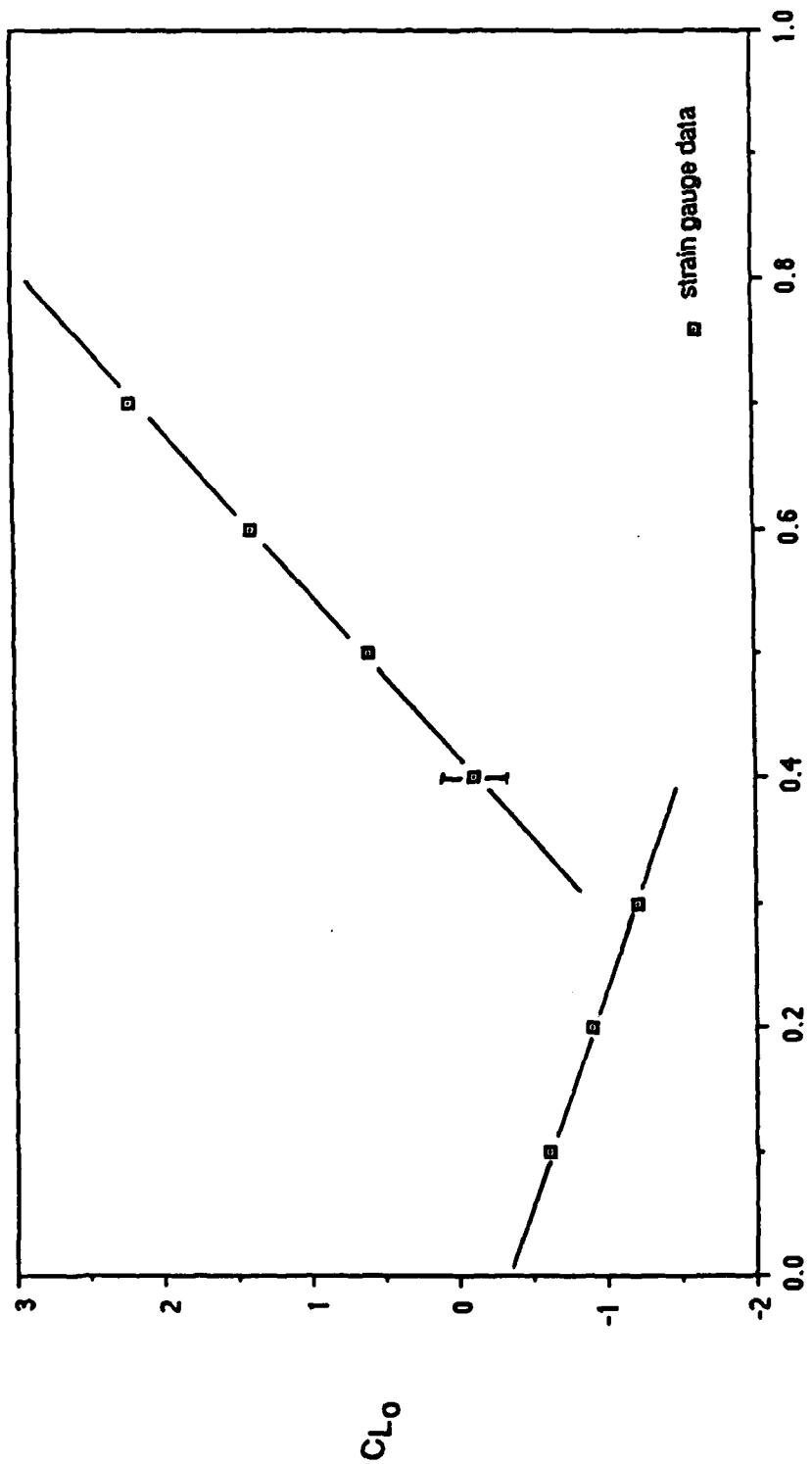

Figure 12. Effect Of Pitching Rate On The Lift Coefficient At The End Of Pitch Down Motion

Figure 13. Flow Visualization During Pitch Down Motion For K=Ø.1, Re=248,ØØØ

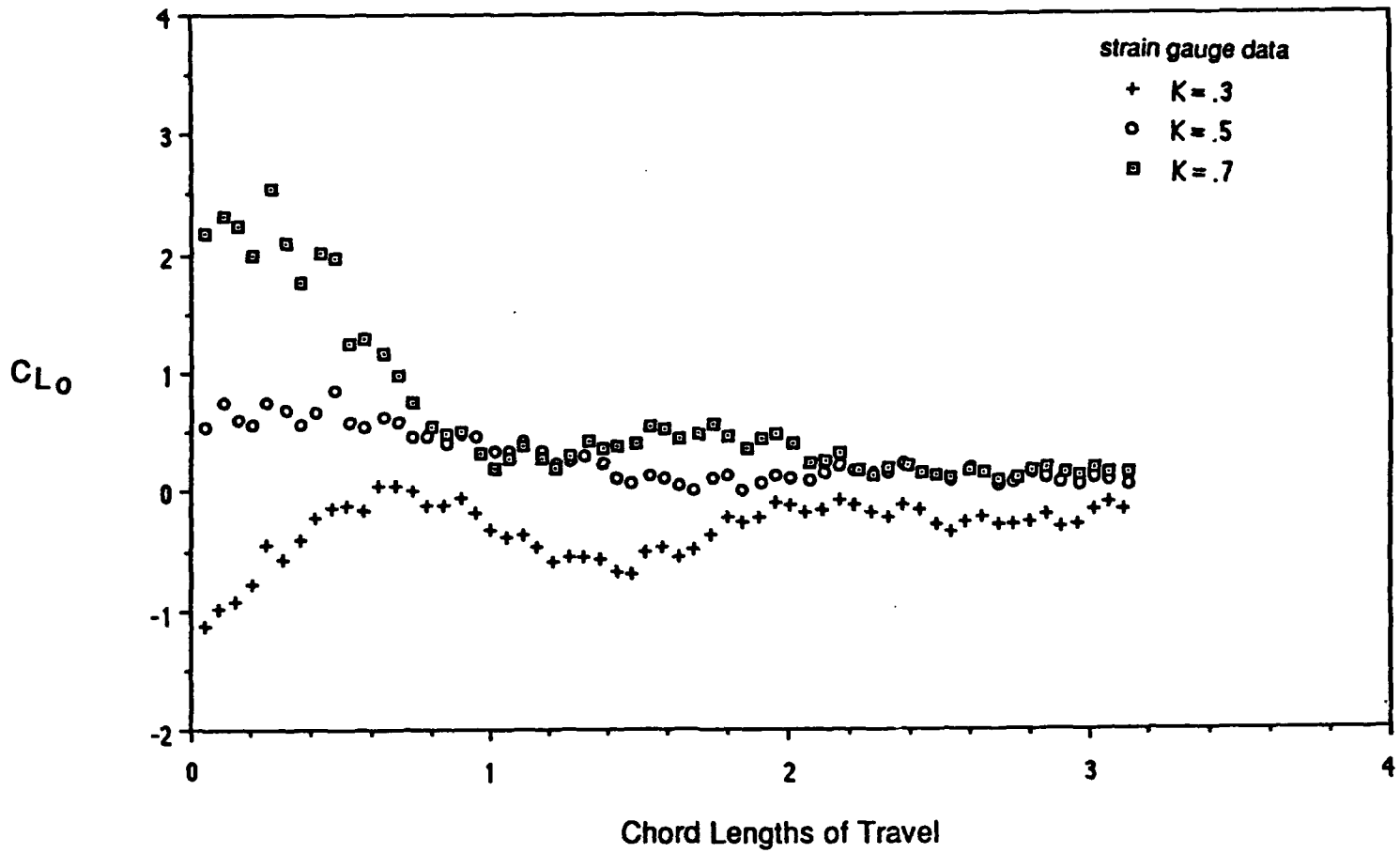

Figure 14. Recovery Of Static Lift At The End Of Pitch Down Motion, Re=248,000

happened in the past. One objective of the present study was to examine when the cessation of the effects of aerodynamic stall occurs. The data of Figure 14 indicate that for the pitching rates considered in this study, the effects of stall persist throughout the pitch down motion and for a significant period of time after the return to a static motion.

3.4 Effect of Pitch Down Inception

The lift and drag forces from the moment the pitch up motion ends are plotted as a function of chord lengths of travel in Figure 15. This figure illustrates the variation in the loading during the period of constant angle of attack at 90 degrees from 0 to 0.25 chords of travel, and the effect of the inception of the pitching down motion. In the case of the lift it can be seen that for K=0.5 and K=0.7 there is a build up of the lift during the constant alpha motion. As the pitch down begins there is an initial loss of lift for the first half chord of travel. Beyond this the lift force grows rapidly. As previously noted, this increase in lift is associated with the large velocity induced by the dynamic stall vortex at the airfoil surface. The data for K= 0.3 show a similar behavior, although not as pronounced. The drag force decreases during the constant alpha motion. With the exception of the case of K=0.7 the inception of the pitching down motion appears to have little effect on the drag other than to cause the drag to remain approximately constant. The data for K=0.7 display large oscillations for reasons not completely understood at this time. However, if these oscillations were due to inertial effects which are polluting the strain gauge signal at the high pitching rates, it would be expected to observe this in the data for K=0.5 as well. This is not the case. Therefore, it would appear that the oscillations are caused by the fluid dynamics of the airfoil-dynamic stall vortex interaction shown in Figure 10.

3.5 Effect of Reynolds Number

Lift forces were measured for three Reynolds numbers of 141,000, 248,000, and 342,000.The results for the nondimensional pitching rate of K=0.2 are shown in Figure 16. As seen here, the Reynolds number has a significant effect on the lift during the pitch up motion. The maximum lift is inversely related to the Reynolds for the range considered here. The Reynolds number appears to have little effect on the lift during the pitch down motion. The effect of Reynolds number on the maximum lift and drag forces during both pitch up and pitch down motions is shown in Figure 17. Also given in this Figure are the data from Reference[3].

3.6 Flow Visualizations

Flow visualizations for the pitching up motion have been presented and discussed in detail in Reference[9]. Therefore, this discussion will focus only on the present results for the pitch down motion. The discontinuity of the lift data in Figure

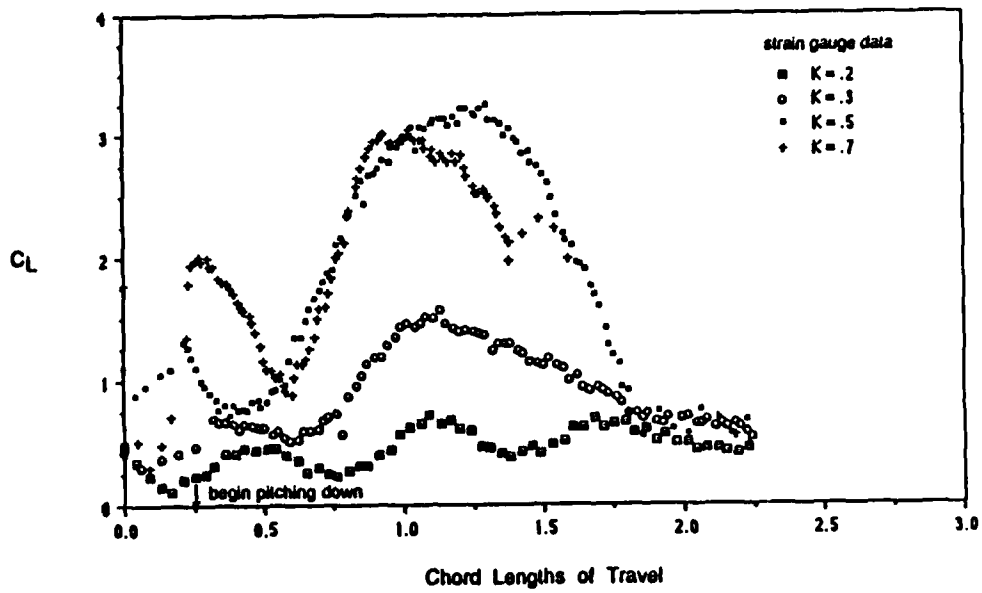

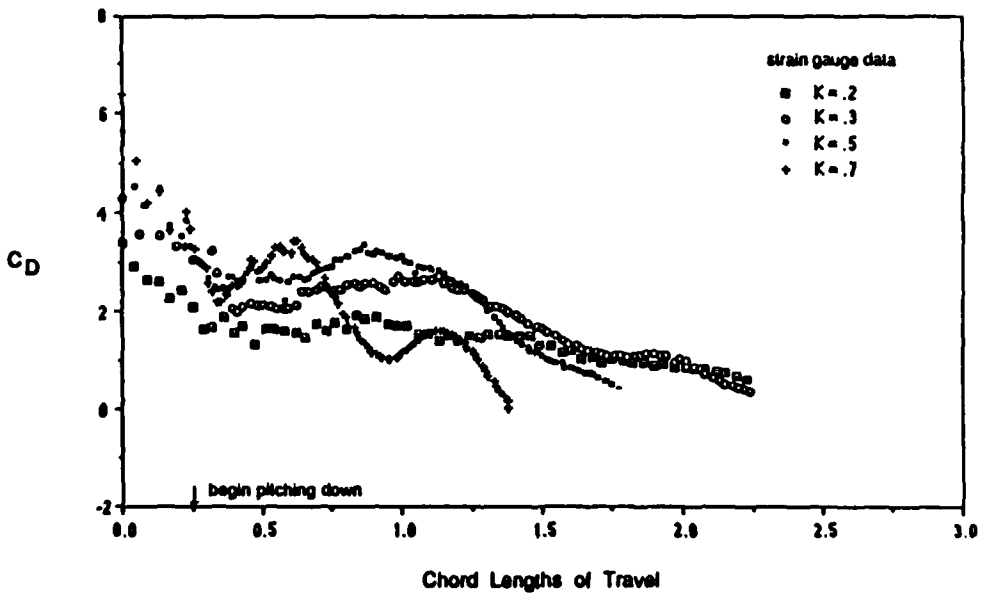

Figure 15. Effect Of Pitch Down Inception On The Force Coefficients, Re=248,000

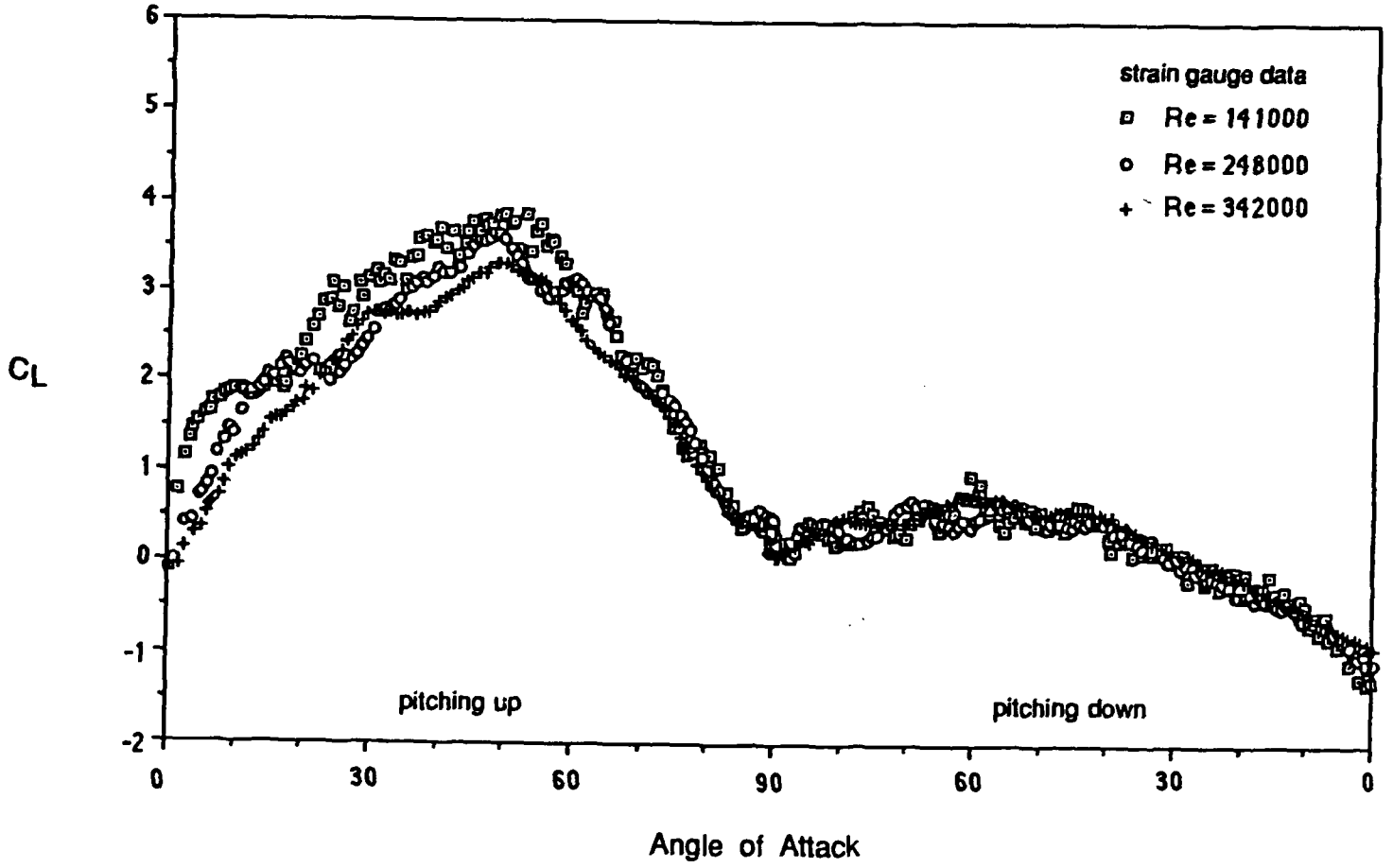

Figure 16. Effect Of Reynolds Number On The Lift For K=Ø.2

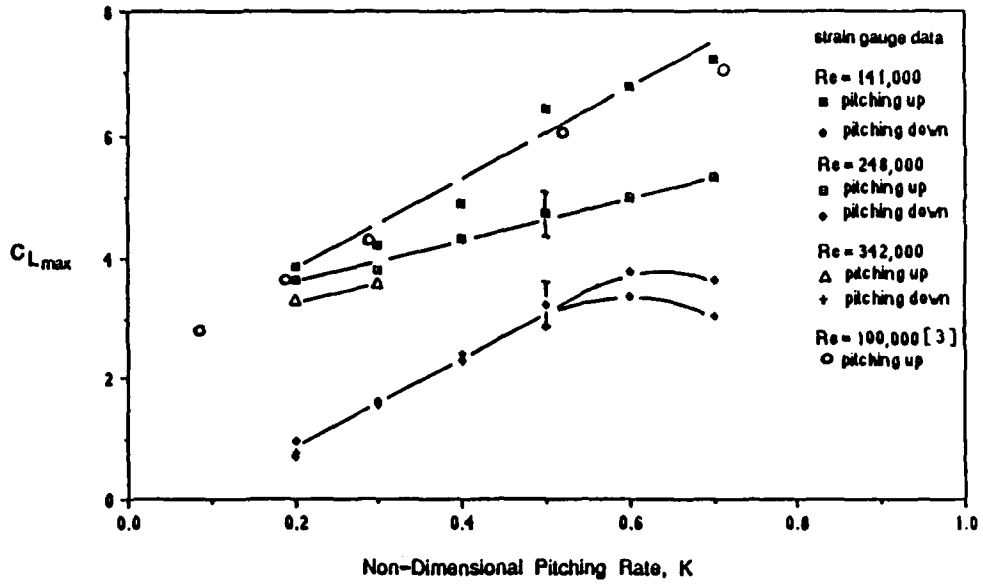

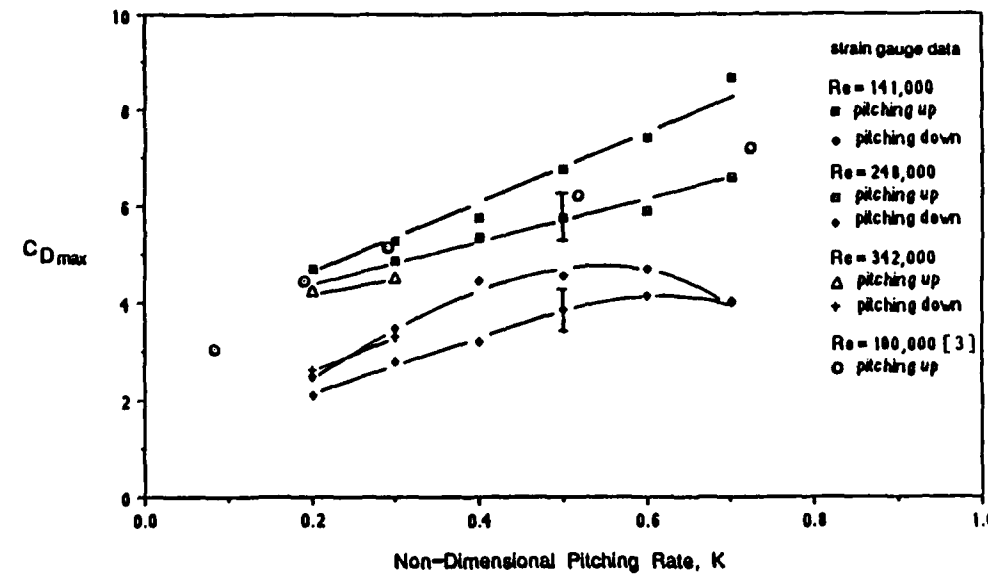

Figure 17. Maximum Lift And Drag Coefficients

12 suggests that there may be dissimilarities in the flows for pitching rates below K= Ø.3 from those above Ø.3. The flow visualizations indicate that a dissimilarity does in fact exist. The principle difference being that at pitching rates below K= Ø.3 the dynamic stall vortex releases from the airfoil surface and in convected and diffused away during the pitch down motion. The result of this is a relatively weak airfoil-vortex interaction. Perhaps the strongest influence of the dynamic stall vortex in this case is that as it convects away from the airfoil surface it appears to create a region of low pressure. Fluid flowing from the trailing edge of the underside of the airfoil initially surges upward into this region of low pressure and then is forced downward toward the upperside of the airfoil. As discussed in Section 3.3, this flow reversal may be the cause of the negative lift coefficients observed at the lower pitching rates. Another interesting aspect of the flow at the lower pitching rates is the diffusion of the dynamic stall vortex.The flow at several instances during the pitch down is shown in Figure 18 for the case of K=Ø.3. As the motion proceeds the dynamic stall vortex expands and the leading edge shear layer appears to coalesce into smaller vortical structures as seen in the photograph at 33 degrees angle of attack. This behavior is also seen in the flow visualization in Figure 1Ø for K=Ø.2. By the time the airfoil reaches Ø degrees angle of attack the dynamic stall vortex has convected downstream beyond the flow visualization field.

Flow visualization data representative of the higher pitching rates(K > Ø.3) are shown in Figure 19 for the pitching rate of K=Ø.5. As seen here, the dynamic stall vortex does not release from the airfoil, but rolls along the airfoil surface towards the trailing edge. The vortex does not convect away from the airfoil, but rather is dispersed by the trailing edge which moves into the vortex. This is seen in the flow visualization at 2Ø degrees angle of attack. It should be noted that this strong airfoil-vortex interaction is related to the specific motion considered here. In other words, if the constant alpha motion is held for longer than Ø.25 chord lengths the dynamic stall vortex will move farther away from the airfoil and may not come in contact with the trailing edge.

3.7 Flow Reattachment

Shown in Figure 2Ø is the flow visualization data for the nondimensional pitching rate of K=Ø.1 at several instances in time during the pitch down motion. The process of flow reattachment begins to take place at an angle of attack of approximately 25 degrees. The onset of reattachment is marked by the shedding of a small vortex which flows along the surface of the airfoil. At an angle of attack of Ø degrees the vortex has not yet reached the trailing edge and there remains a significant region of separated flow. This type of reattachment was observed at pitching rates of K=Ø.2 and K=Ø.3 as well. For pitching rates above K=Ø.3 the inception of boundary layer reattachment was observed to take place only after the pitch down motion had ended and the airfoil had moved several chord lengths.

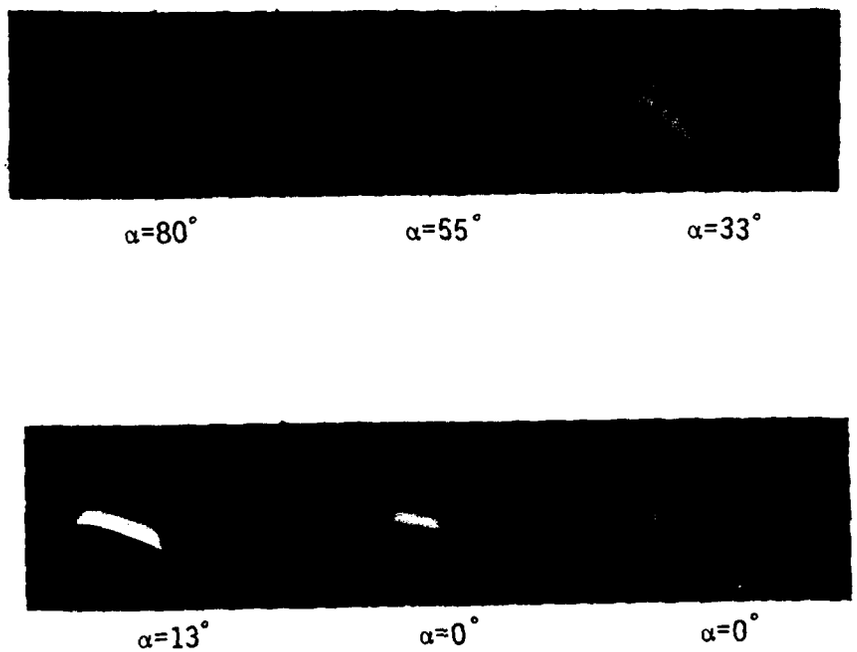

Figure 18. Flow Visualization During Pitch Down Motion For K=Ø.3, Re=248,ØØØ

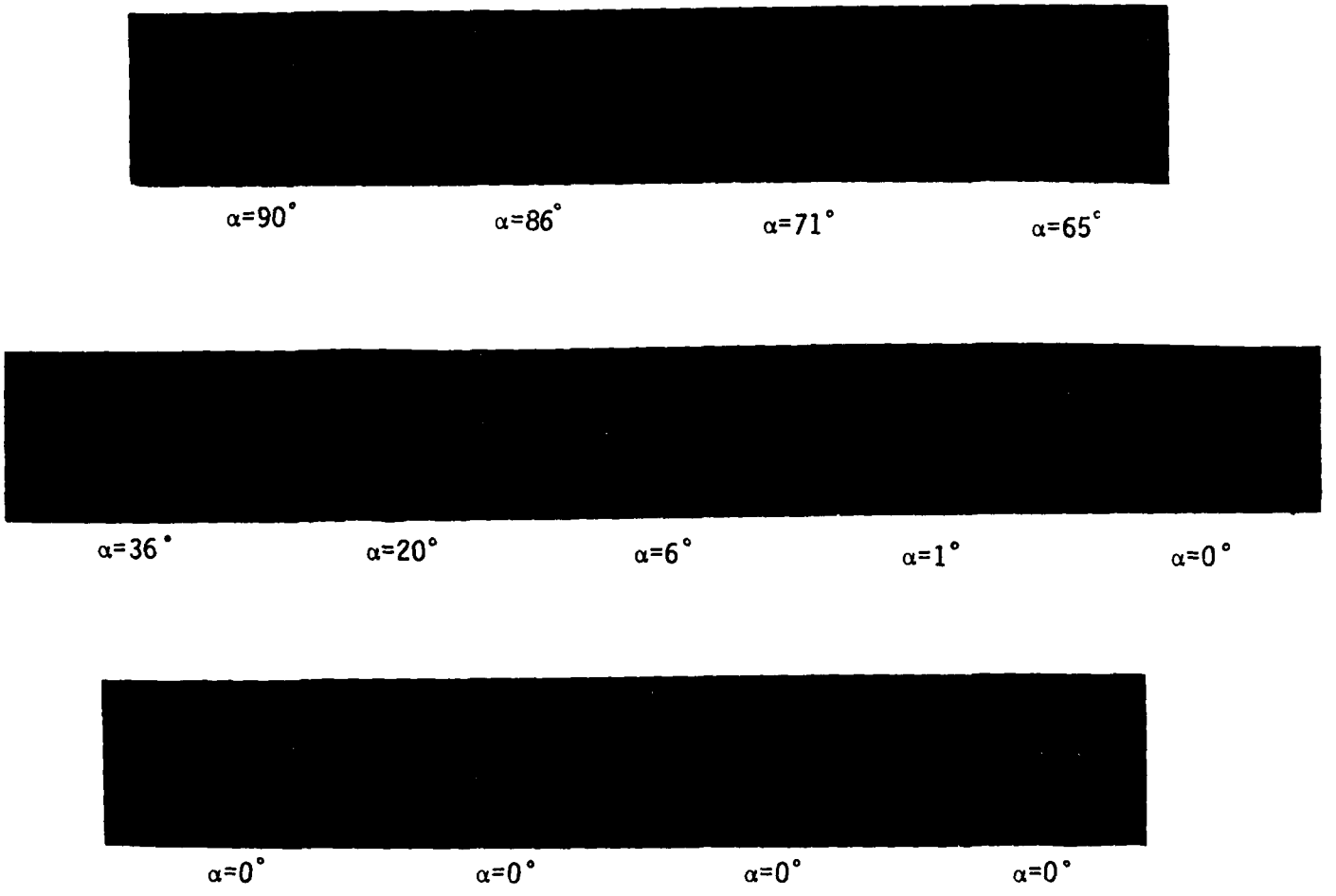

Figure 19. Flow Visualization During Pitch Down Motion For K=Ø.5, Re=248,ØØØ

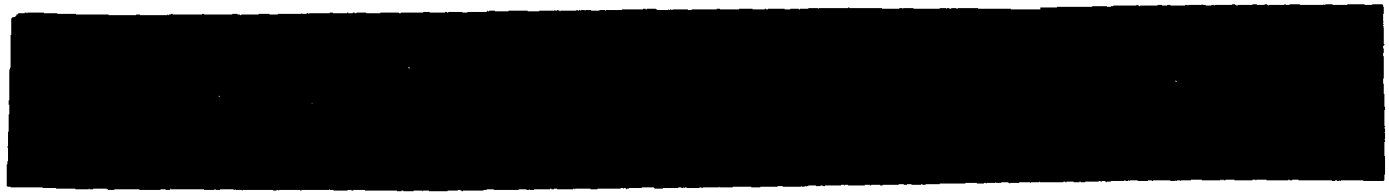

Figure 2Ø. Flow Reattachment During Pitch Down Motion For K=Ø.1, Re=248,ØØØ

3.8 Underside Flow

Flow visualizations were obtained on the underside of the airfoil to determine whether underside boundary layer separation occurs as the pitch up motion begins. The possibility of underside separation arises when considering the large negative effective angle of attack at the leading edge at the inception of the pitch up motion. For the case of K=Ø.7 the effective nose angle of attack at Ø degrees geometric angle of attack for an airfoil pitching about the quarter chord is -19.29 degrees. The underside flow for K=Ø.7 at an angle of attack of 15 degrees is shown in Figure 21. There appears to be no significant separation, or remnants of previous separation in this flow visualization. Similar results were obtained at the lower pitching rates considered here.

4. Conclusion

The present study has shown the variation in airfoil loading for a complete two dimensional post stall maneuver. The airfoil loading during the pitch down sequence has been shown to be related to the airfoil-dynamic stall vortex interaction. For pitching rates below K=Ø.3 this interaction results in negative lift coefficients. At higher pitching rates it has been shown that the interaction produces large lift forces during the pitch down motion. The effects of aerodynamic stall have been observed to persist throughout the pitch down motion and into the subsequent static motion for several chord lengths. Finally, the possibility of underside flow separation has been investigated. Underside separation was not observed at the highest pitching rate considered here.

5.Acknowledgments

The author acknowledges the support of the AFOSR under Grant No. AFOSR-87-Ø312.

6. References

1.Lorber,P. and Carta,F., "Airfoil Dynamic Stall at Constant Pitch Rate and High Reynolds Numbers," Journal of Aircraft, June 1988.

2.Jumper,E., Schreck,S., and Dimmick,R., "Lift-Curve Characteristics for an Airfoil Pitching at Constant Rate," Journal of Aircraft, Oct.1987.

3.Strickland,J. and Graham,G.,"Force Coefficients on a NACA ØØ15 Airfoil Undergoing Constant Pitch Rate Motions," AIAA Journal, April 1987.

α=15°

Figure 21. Underside Flow During Pitch Up Motion For K=Ø.7, Re=248,ØØØ

4.Walker,J., Helin,H., and Strickland,J., "An Experimental Investigation of an Airfoil Undergoing Large Amplitude Pitching Motions," AIAA Journal, Aug.1985.

5.Carr,L., "Progress in the Analysis and Prediction of Dynamic Stall," Journal of Aircraft, Jan.1988.

6.Herbst,W., "Supermaneuverability," AFOSR/FJSRL/ Univ.of Colo. Workshop on Unsteady Separated Flow, Colo.Sprgs., Colo., Aug.1983.

7.Yeow,K., "An Experimental Investigation of High Lift/High Rate Aerodynamics of an Unsteady Airfoil," Master's Thesis, Ohio Univ., Athens, Oh., March 1989.

8.Tobak, M. and Schiff, Q., "Aerodynamic Mathematical Modeling-Basic Concepts," AGARD Lecture Series No.114, Paper 1, March 1981.

9.Graham,G., "An Experimental Investigation of an Airfoil Pitching at Moderate to High Rates to Large Angles of Attack," Doctoral Dissertation, Texas Tech Univ., Dec.1985.

Appendix: Force Coefficients

This appendix contains a complete set of lift and drag force data measured in this study. The data are for a NACA ØØ15 airfoil undergoing the motion shown in Figure 2 in the body of this report. The data are for an airfoil pitching about the quarter chord. The nondimensional pitching rate($K= \dot{\alpha}C/2U_\infty$) and the Reynolds number(Re) are indicated at the bottom of each figure. The data for K= Ø.1, Ø.3 and Ø.7 at Re=248,ØØØ are given in Section 3.1 and are not reproduced here.

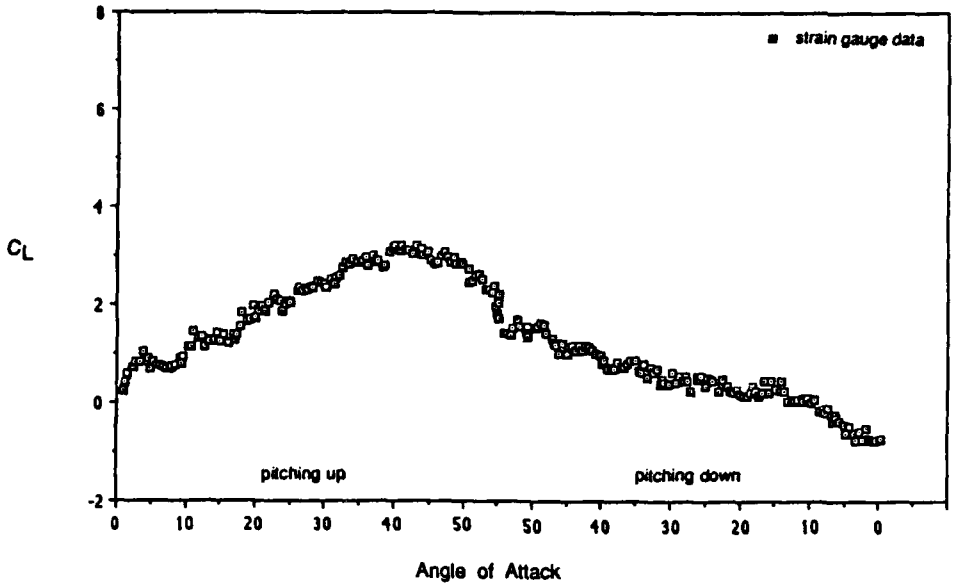

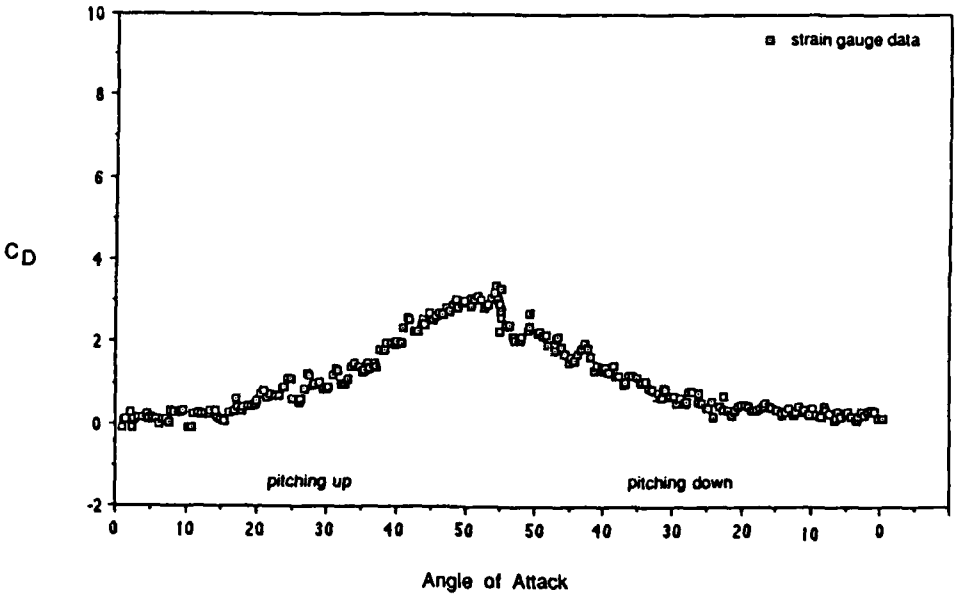

K=Ø.1, Re=141,ØØØ

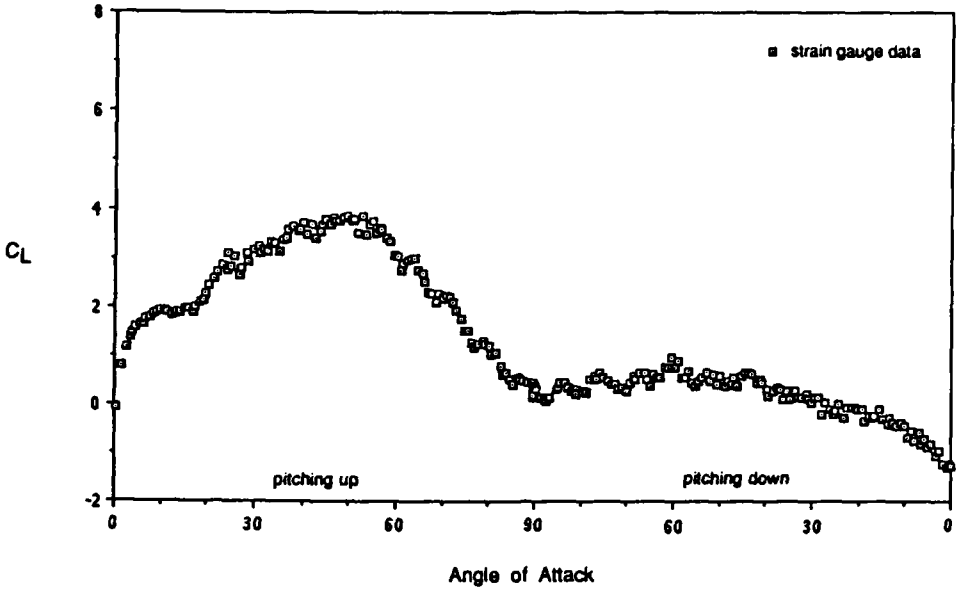

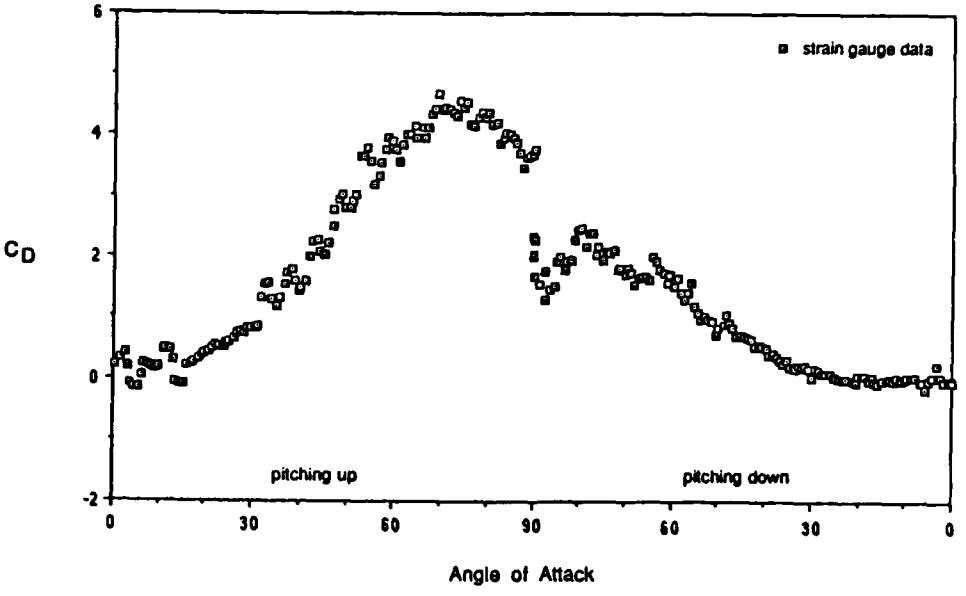

K=Ø.2, Re=141,ØØØ

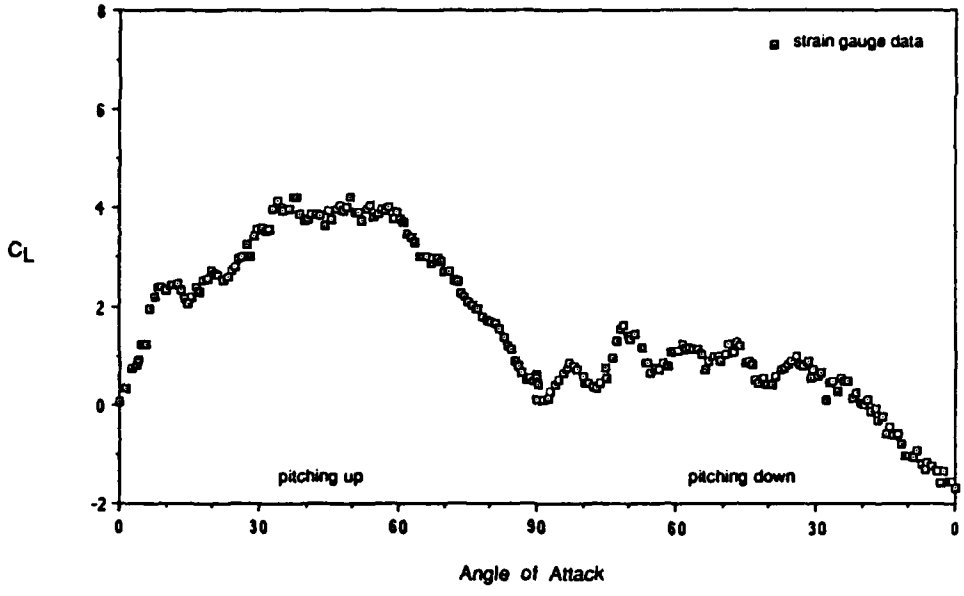

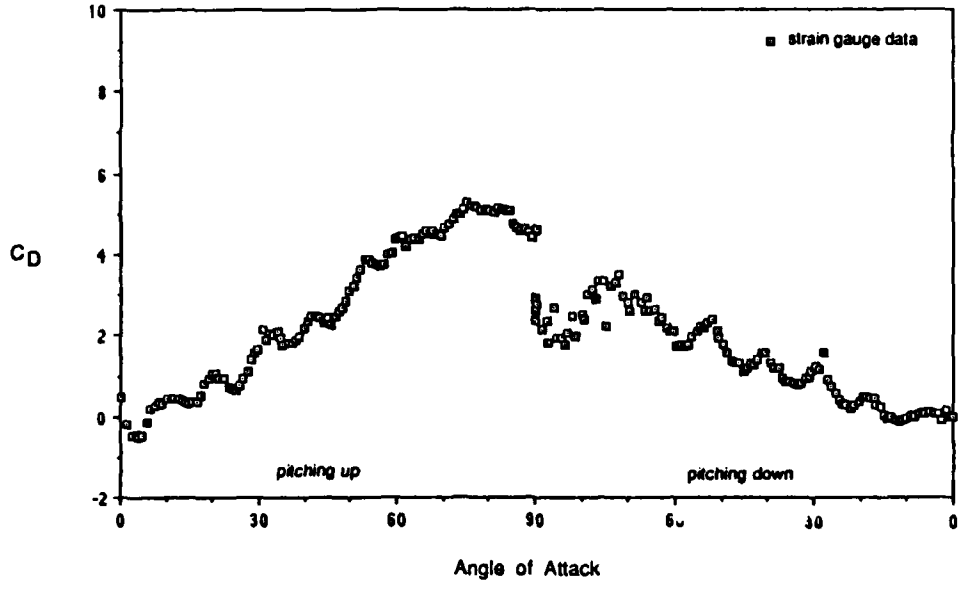

K=Ø.3, Re=141,ØØØ

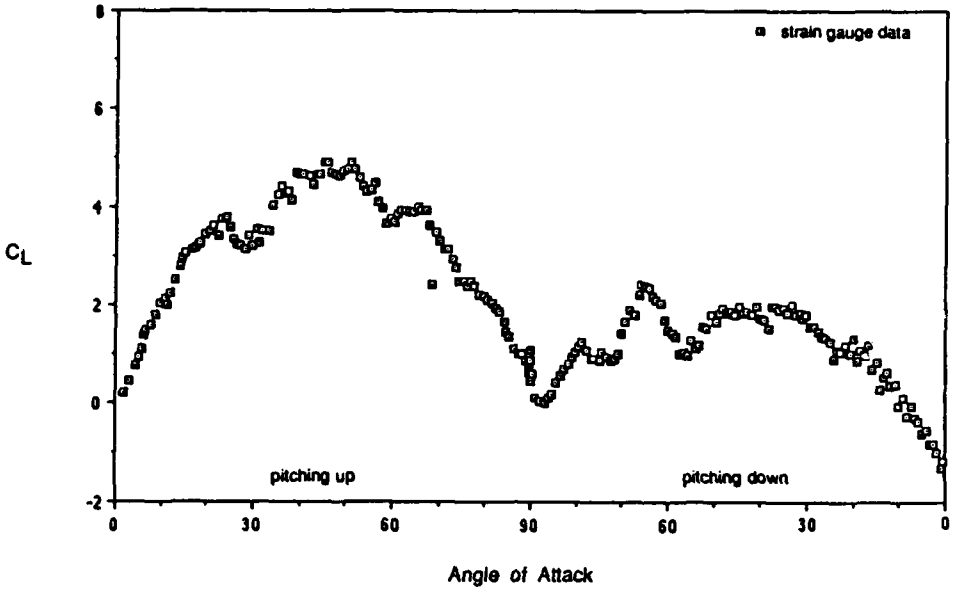

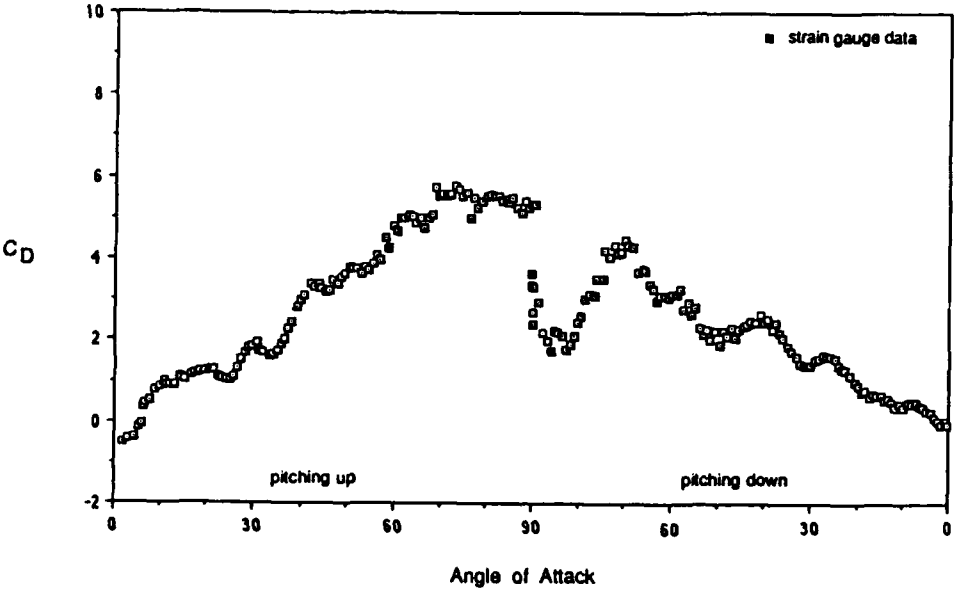

K=Ø.4, Re=141,ØØØ

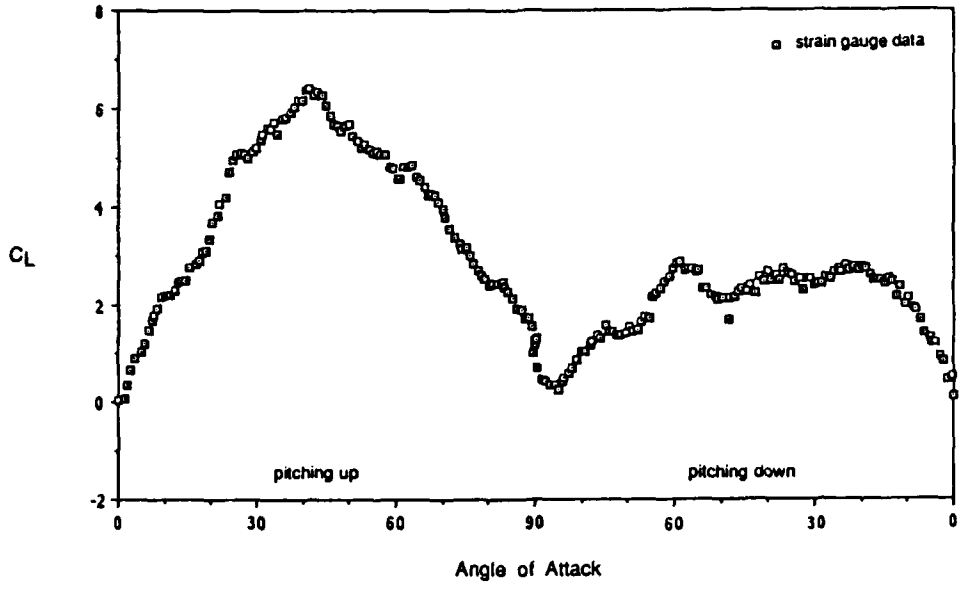

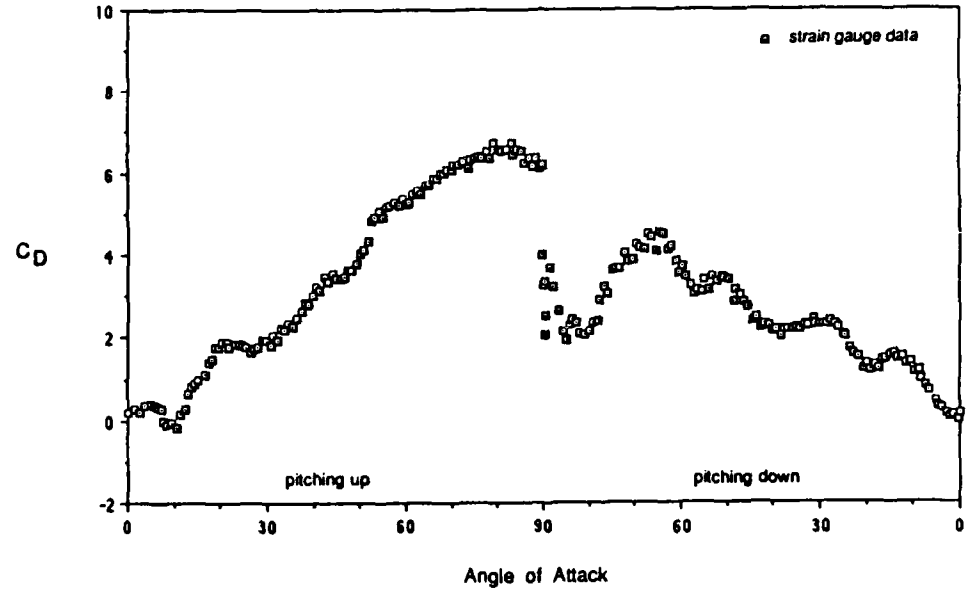

K=Ø.5, Re=141,ØØØ

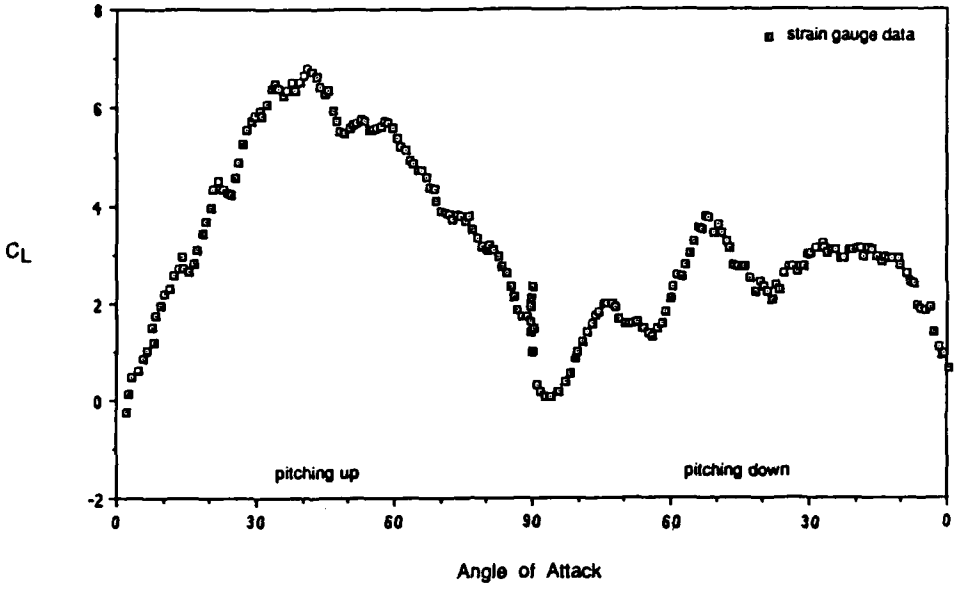

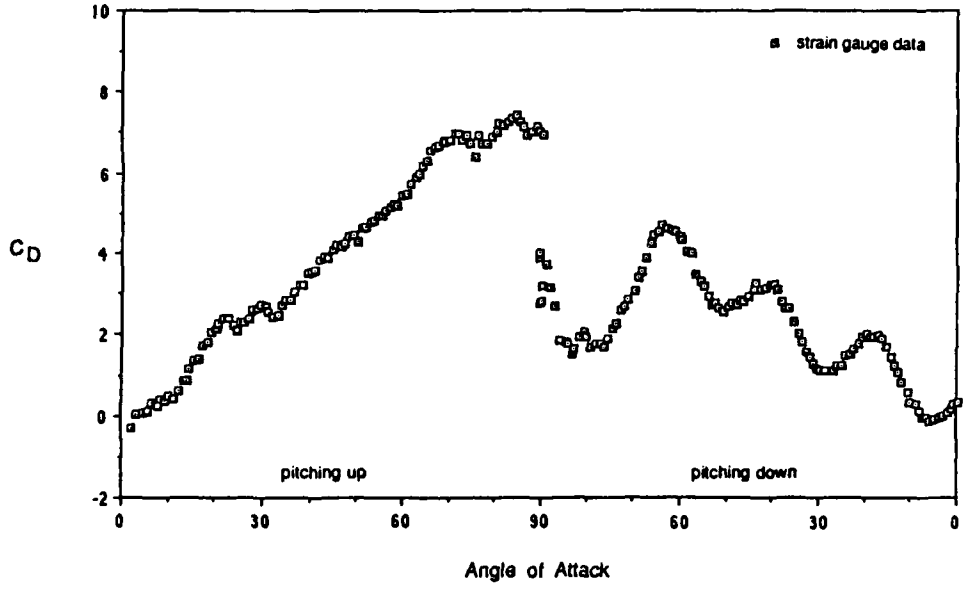

K=Ø.6, Re=141,ØØØ

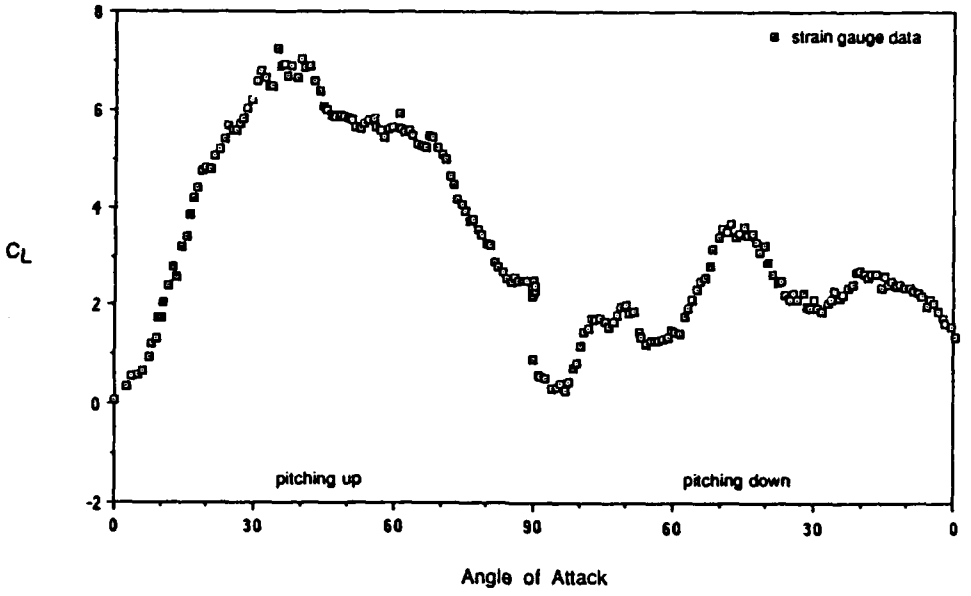

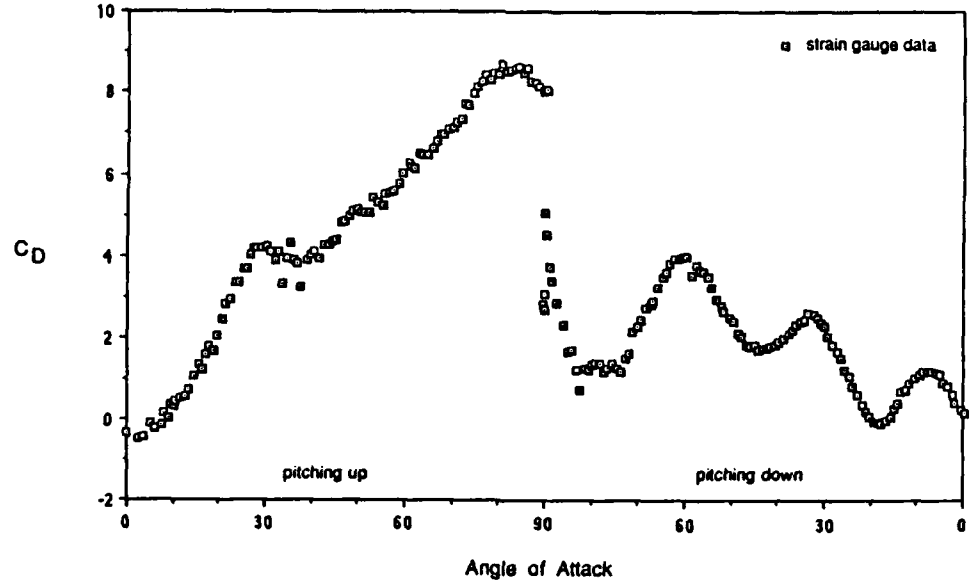

K=Ø.7, Re=141,ØØØ

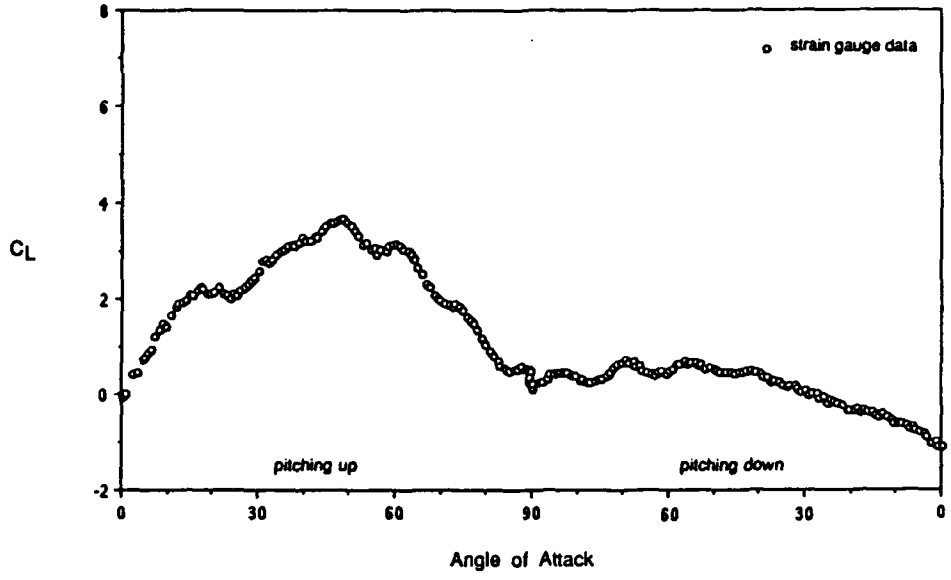

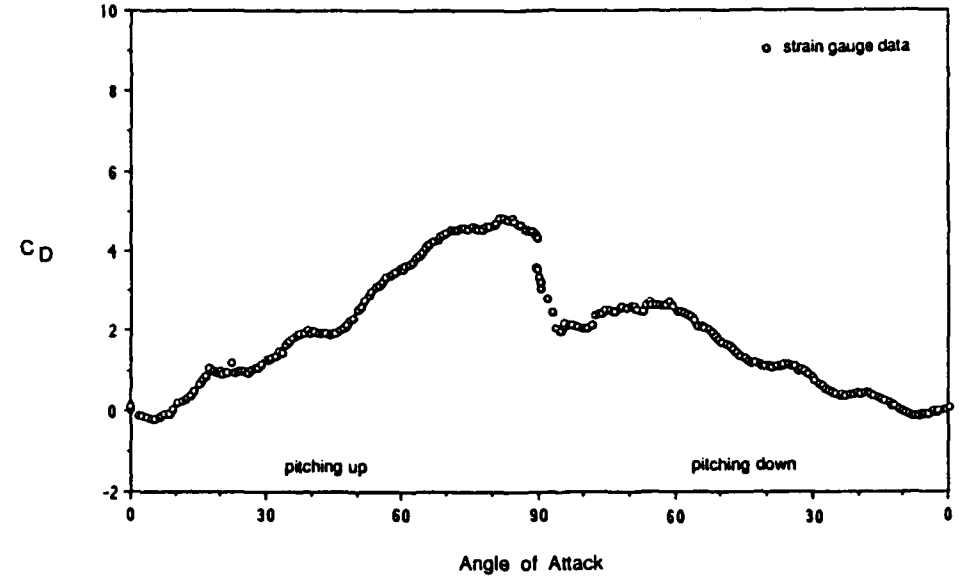

K=Ø.2, Re=248,ØØØ

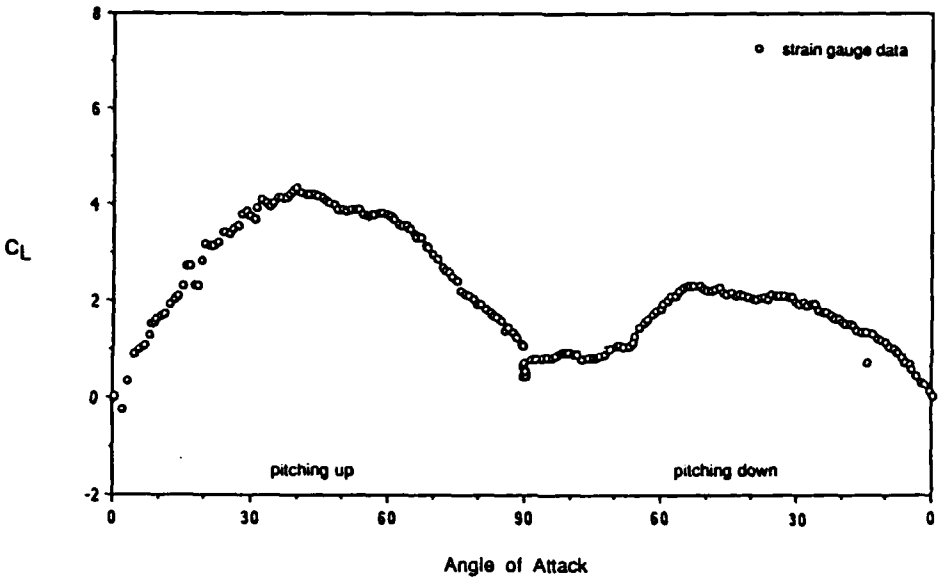

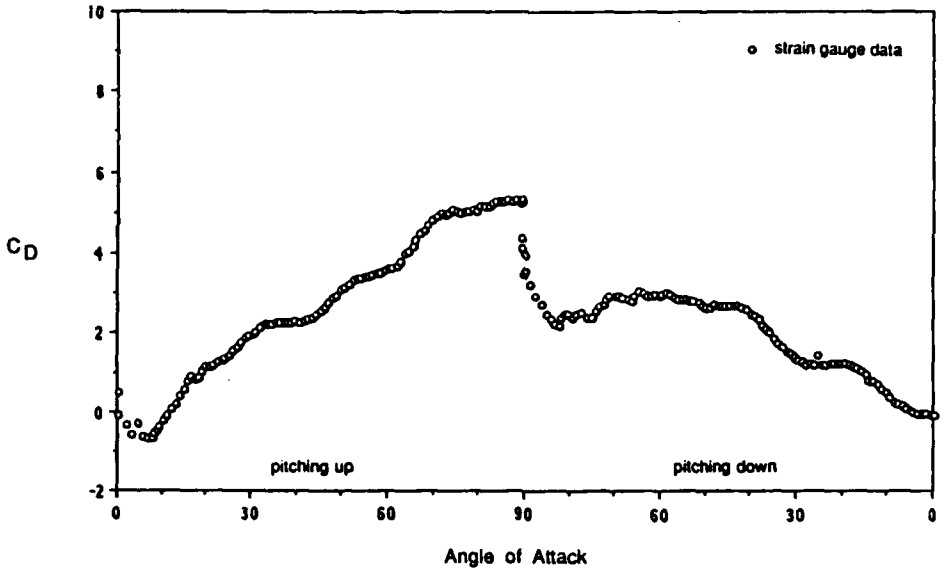

K=Ø.4, Re=248,ØØØ

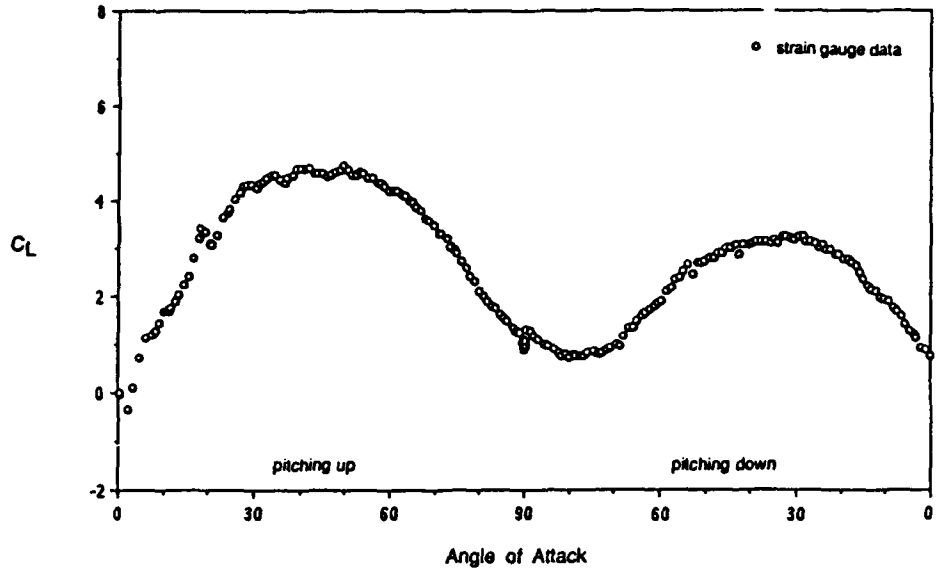

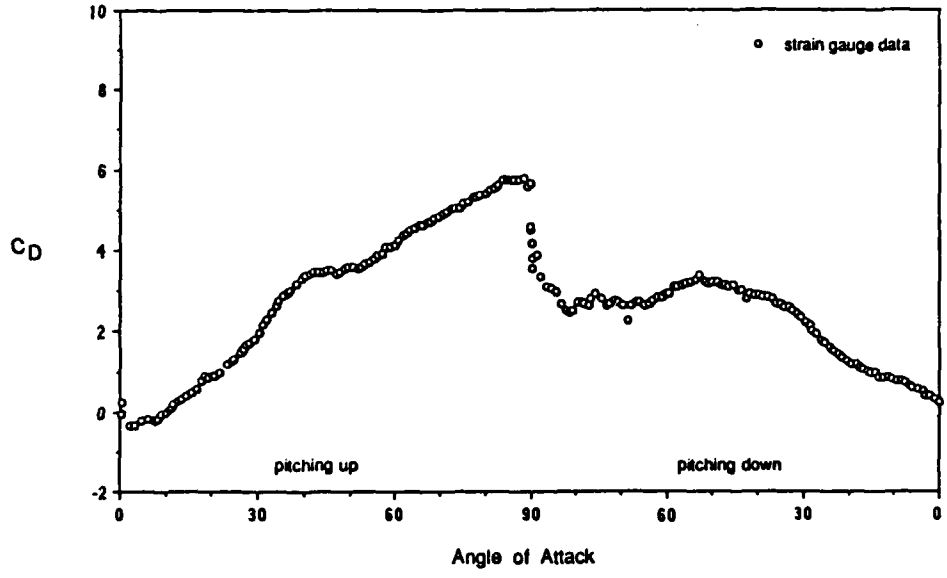

K=Ø.5, Re=248,ØØØ

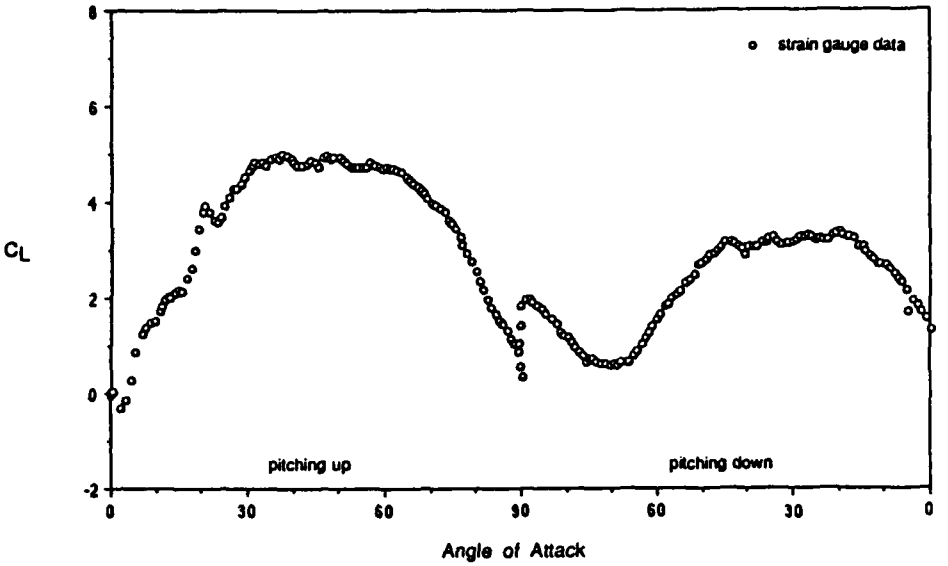

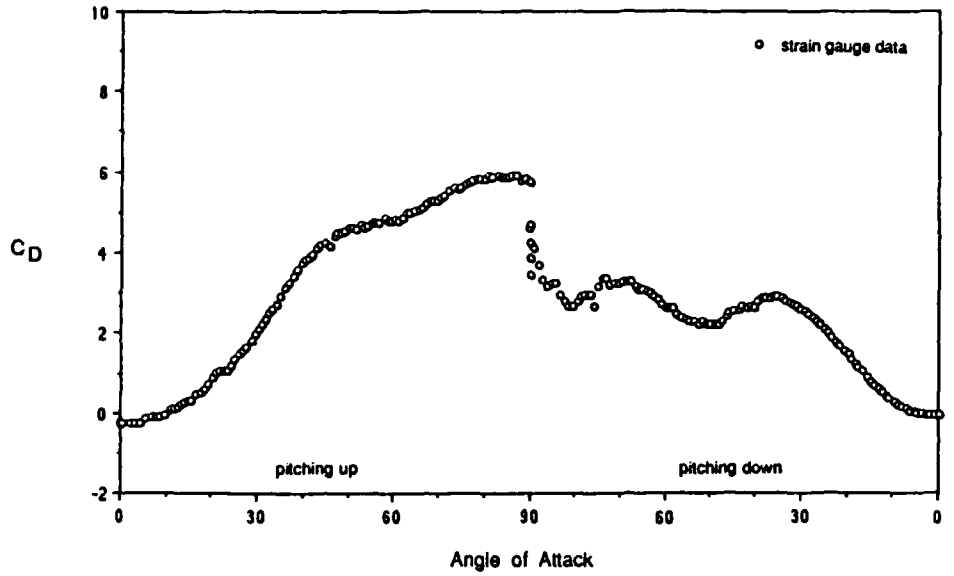

K=Ø.6, Re=248,ØØØ

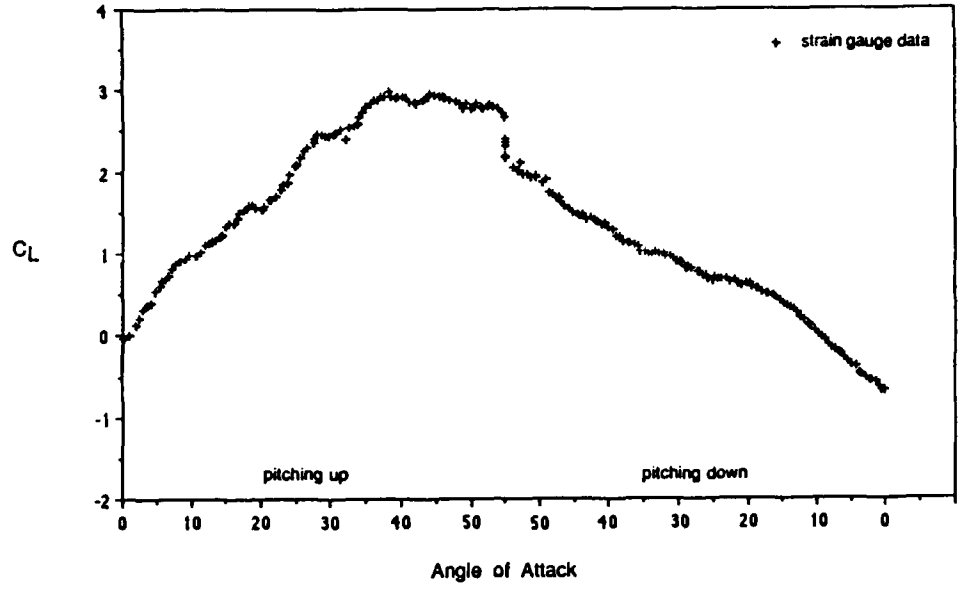

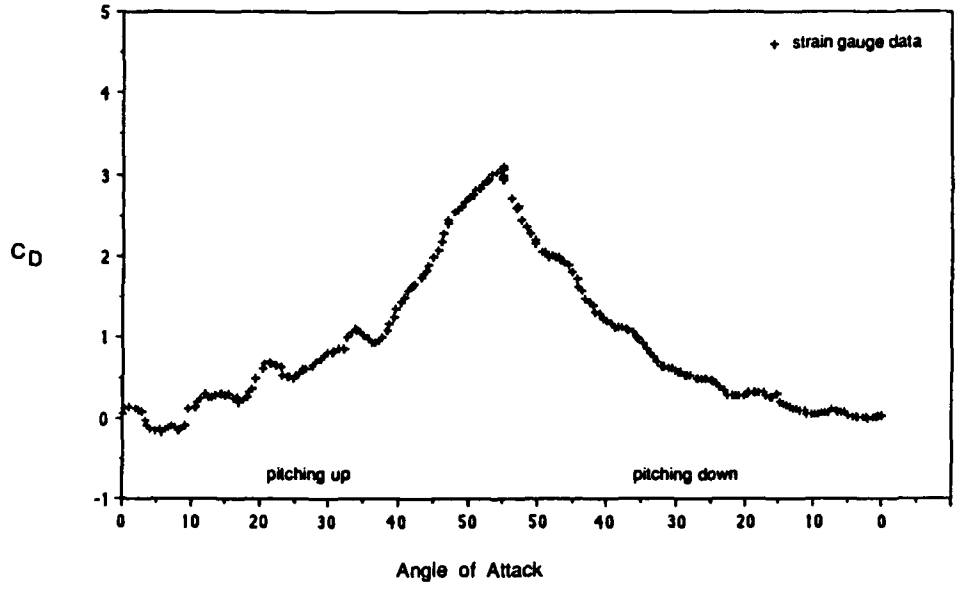

K=Ø.1, Re=342,ØØØ

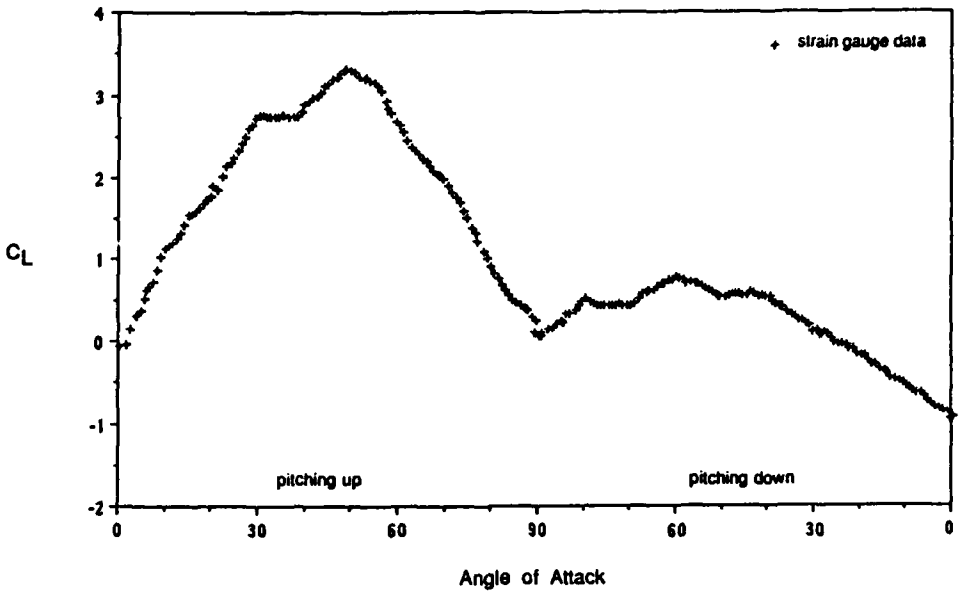

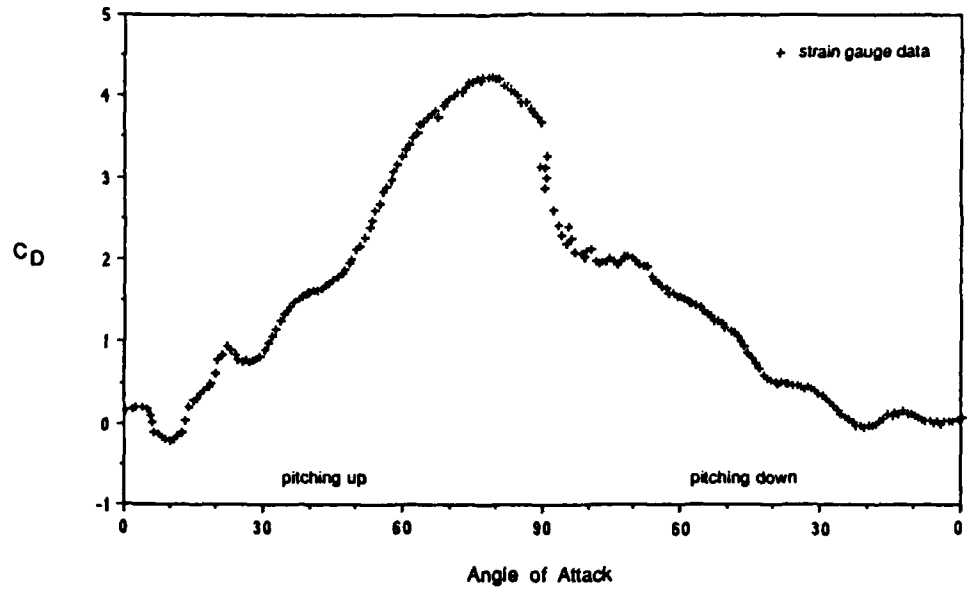

K=Ø.2, Re=342,ØØØ

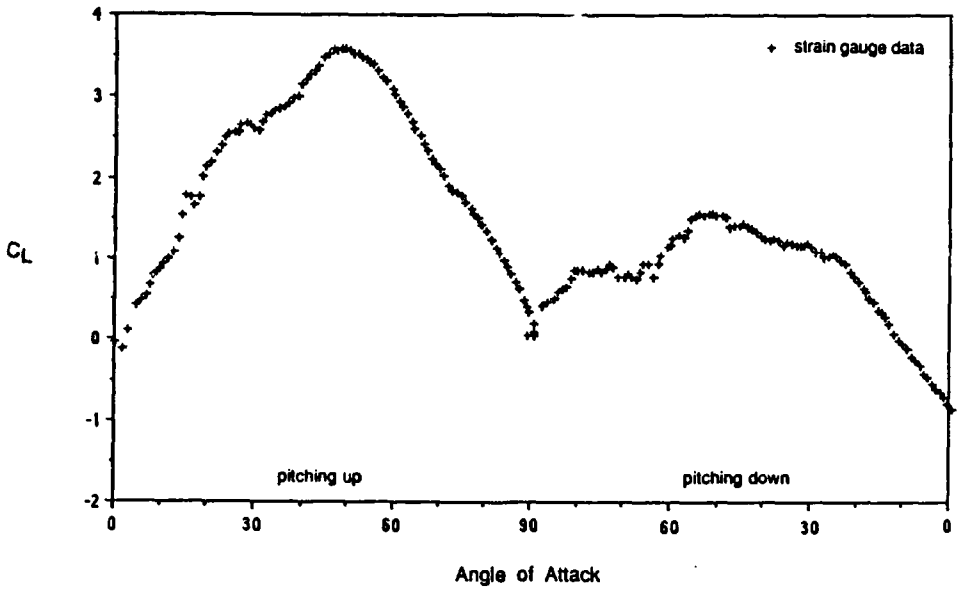

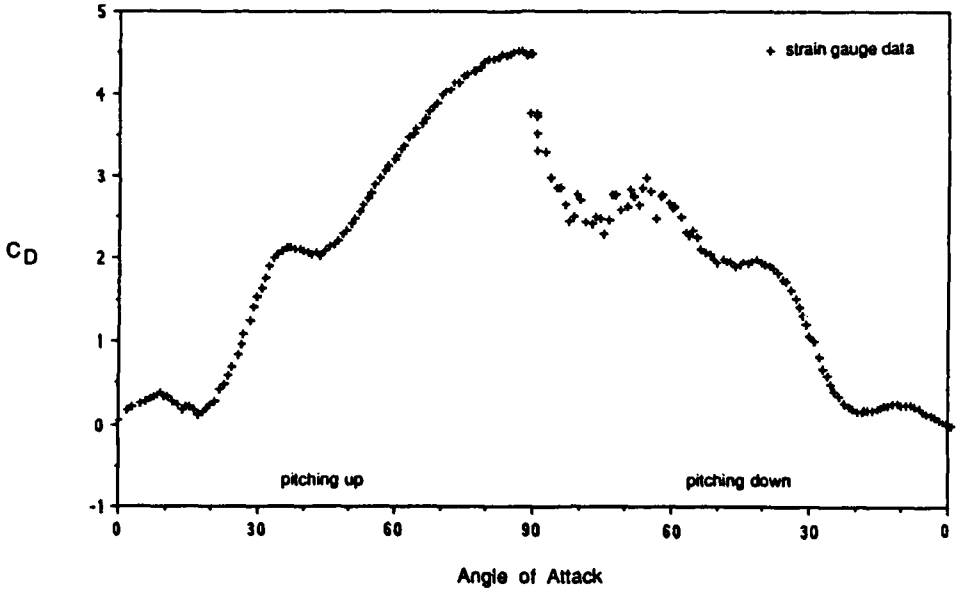

K=Ø.3, Re=342,ØØØ